Journal of the Indian Institute of Science
A Multidisciplinary Reviews Journal
ISSN: 0970-4140 Coden-JIISAD
© Indian Institute of Science

REVIEWS

Electrochemistry of Nanostructured Materials: Implementation in Electrocatalysis for Energy Conversion Applications

Srabanti Ghosh and Rajendra N. Basu

Abstract | The study of electrochemical phenomena and electrocatalytic properties using chemical structures at nanoscale is a rapidly emerging area in electrochemical and material science. A notable achievement in the performance of functional materials has been the understanding of the electrochemical mechanisms and the development of advanced catalytic nanostructured materials. Consequently, efforts will continue to synthesise and explore novel nanoscale materials to meet the requirement of sustainable and renewable resources owing to climate change and the decreasing availability of fossil fuels. The present review explores in depth the current state of the nanoscale frontier in electrochemistry. It includes investigation of electrochemical processes of nanostructured materials, electroanalysis using nanostructured materials, fundamental aspects of electron transfer and mass transfer at nanoscale surface during catalysis. It will also provide an understanding of the activity and stability of electrocatalysts under critical experimental conditions. A brief discussion on the utilisation of nanostructured materials in energy domains such as fuel cells is presented at the end.

CONTENTS

1 Introduction

Advanced functional materials have now reached the centre stage in the field of green and sustainable energy technology where electrochemistry plays a vital role in grasping the electrochemical phenomena as well as electrocatalytic properties at nanoscale for such high-end applications.[1,2] Electrochemical devices such as fuel cells, storage devices are emerging day by day and nanostructured materials, which offer improved performance to those devices with electrochemical reactions and heterogeneous catalysis, are favoured.[3] Materials at nanoscale dramatically alter the surface property as well as electrical transport offering huge improvement in energy storage, conversion and generation.[4,5] Advancements in electrochemistry provide in-depth understanding of the electrochemical processes involved in the operation of electrochemical cells, which are crucial in the development of new and efficient devices for energy conversion.[6] Modern concepts of interface structure show that adsorbate layers and the edges of surface atoms on electrodes are

Fuel Cell and Battery Division, CSIR-Central Glass and Ceramic Research Institute, 196, Raja S.C. Mullick Road, Kolkata 700032, India.
ghosh.srabanti@gmail.com, rnbasu@cgcri.res.in

spatially separated by gaps, which depend on electrode potential (charge). Moreover, electrode surfaces are in contact with electrolyte, the so-called electrified interfaces in electrodics, metal or semiconductor electrolyte junctions, whose properties can be controlled via charge transfer length and charge transfer kinetics.[7,8] Consequently, there is an urgent need to differentiate between the electrochemical processes that arise from charge transfer length relating to the surface properties of nanoscale materials and transport properties through nanostructures. Furthermore, charge transfer kinetics is also influenced by high surface area of nanomaterials, which provide large number of electroactive charge transfer sites. The objective of the review is to examine how the fundamentals of electrochemical analysis and the most relevant properties of nanostructured materials improve the alternative energy devices. Specifically, the review presents an overview of the basic principles of electrochemistry governing the effects of nanoscale structures of electrodes and electrolytes, electrochemical characterisation of nanostructure electrodes as well as their application in energy conversion and electrocatalysis. It also illustrates the morphology, electrical properties, oxidation kinetics, and electrochemical parameters of materials for energy applications and how nanostructured materials can modify the performance of electrocatalyst materials.

2 Fundamentals of Electrocatalytic Reactions

To understand how nanomaterial is useful to electrochemical energy devices, an understanding of the fundamental principles of electrochemical generation is necessary. Energy gets converted through energy transfer at a finite rate at an interface. Hence, the performance of an electrochemical device depends on the efficiency of reaction occurrence and the surface of the reaction through which electronic transfer, transport and kinetic reactions take place. The electrochemical oxidation of hydrogen and small organic molecules such as ethanol, methanol, formic acid, glucose has been studied extensively in the context of their utilisation in these reactions in low-temperature fuel cells.[9–11] Among the various types of fuel cells, proton-exchange membrane fuel cells (PEMFCs) and direct alcohol fuel cells (DAFCs) are now approaching the stage of commercialisation for use in automotive and portable electronic applications.[12,13] A PEMFCs consists of an anode, a cathode and an electrolyte (proton-conducting membrane).[14] The anode and cathode are normally bonded to the membrane electrolyte and de-ionised water is supplied to the anode where it splits into proton, electron and oxygen in the presence of a catalyst. The proton moves through the proton-exchange membrane (PEM) to the cathode and electrons through external circuit. Figure 1 illustrates the operating principles of PEMFCs that use hydrogen as a fuel and oxygen as an oxidant. The H^+ ions produced by an electrocatalytic oxidation of H_2 gas by the Pt catalyst migrate from anode to cathode through proton-conducting Nafion membrane. The electrons however flow through the external circuit from anode to cathode, where they electrocatalytically reduce, with assistance from the Pt catalyst, O_2 gas to O_2^- ions to combine with H^+ ions to produce water. The overall reaction is the splitting of two moles of water to produce two moles of H_2 and one mole of oxygen as in equation (1–3).

$$\text{Anode} \quad 2H_2O \rightarrow 4H^+ + O_2 + 4e^- \tag{1}$$

$$\text{Cathode} \quad 4H^+ + 4e^- \rightarrow 2H_2 \tag{2}$$

$$\text{Overall reaction} \quad 2H_2O \rightarrow 2H_2 + O_2 \tag{3}$$

Even though the thermodynamic potential for water electrolysis is 1.23 V, the kinetics of the reaction restricts the reaction and an additional potential called overpotential has to be applied for the reaction to occur.[15] The selection of overpotential depends on the catalytic material used, to yield low overpotential.[16] In the electrolyser mode, hydrogen evolution reaction (HER) and oxygen evolution reaction (OER) occur for energy storage, while, in the fuel-cell mode, oxygen reduction reaction (ORR) takes place for energy conversion.[17] Both HER and OER require a catalyst for the reaction to occur. However, the present review focusses on the fundamentals of specific electrochemical reactions based on energy conversion and their relationship with nanostructures, which are of vital importance in electrochemical energy conversion devices.

Oxygen reduction is a series of complex electrochemical reactions, which involve multistep electron-transfer processes and complicated oxygen-containing species such as O, OH, O_2^-, HO_2^-.[18] The ORR in alkaline environments at ambient temperature is more favourable than in acidic environments because of better kinetics and lower overpotentials.[19] Oxygen can be directly reduced to water with the concomitant

PEMFC: The proton exchange membrane fuel cell (PEMFC) uses a water-based, acidic polymer membrane as its electrolyte and operate at relatively low temperatures (below 100 degrees Celsius).

consumption of four electrons per O_2 molecule (equation 4). Alternatively, oxygen can be reduced indirectly, forming H_2O_2 as an intermediate and only two electrons per O_2 molecule are consumed (equation 5):

$$O_2 + 2H_2O + 4e^- \rightarrow H_2O + 4\ OH^- \quad \left(E^0 = 0.40\ V\right) \tag{4}$$

$$O_2 + H_2O + 2e^- \rightarrow H_2O_2 + 2\ OH^- \left(E^0 = -0.07\ V\right) \tag{5}$$

$$HO_2^- + H_2O + 2e^- \rightarrow 3OH^- \qquad \left(E^0 = 0.87\ V\right) \tag{6}$$

$$HO_2^- \rightarrow 3OH^- + O_2 \tag{7}$$

Oxygen reduction may proceed via a four- ($4e^-$) or a two-electron ($2e^-$) pathway on metal surfaces. The overall electron transfer numbers per oxygen molecule involved in the typical ORR process were calculated from the slopes of the Koutecky-Levich plots using the following equation:[20]

$$\frac{1}{j} = \frac{1}{j_L} + \frac{1}{j_K} = \frac{1}{B\omega^{\frac{1}{2}}} + \frac{1}{j_K} \tag{8}$$

$$B = 0.62\ nFC_0 \left(D_0\right)^{\frac{3}{2}} \nu^{-\frac{1}{6}} \tag{9}$$

$$j_K = nFk\ C_0 \tag{10}$$

where, j (mA/cm^2) is the measured current density, j_K and j_L (mA/cm^2) are the kinetic- and diffusion-limiting current densities, ω, the electrode rotating speed in rpm, n, the number of electrons transferred per oxygen molecule, F, the Faraday constant ($F = 96485\ C\ mol^{-1}$), C_0, the bulk concentration of O_2 ($1.2 \times 10^{-6}\ mol\ cm^{-3}$), D_0, the diffusion coefficient of O_2 ($1.9 \times 10^{-5}\ cm^2\ s^{-1}$), ν, the kinematic viscosity of the electrolyte ($0.01\ cm^2\ s^{-1}$), and k, the electron transfer rate constant.[21] In particular, the electrooxidation of ethanol has been a subject of increasing interest; however, the kinetics of alcohol oxidation are much slower than that of hydrogen oxidation reaction. In alkaline condition, oxidation of ethanol generates 12 e^- (equation):

$$\text{Anode,}\quad CH_3CH_2OH + 12OH^- \rightarrow 2CO_2 + 9H_2O + 12e^- \tag{11}$$

$$\text{Cathode,}\quad 3O_2 + 6H_2O + 12e^- \rightarrow 12OH^- \tag{12}$$

Moreover, ORR at cathode is basically diffusion-limited, while electrooxidation of liquid fuel such as ethanol, methanol at anode is primarily catalytically driven (Figure 1).

Koutecky–Levich (KL) plot: KL plot is based on the extrapolation of the reciprocal of the current intensity (or density) versus the reciprocal of the square root of the rotational rate of a rotating disc electrode (plot 1/j vs ω − 1/2) for different applied potentials.

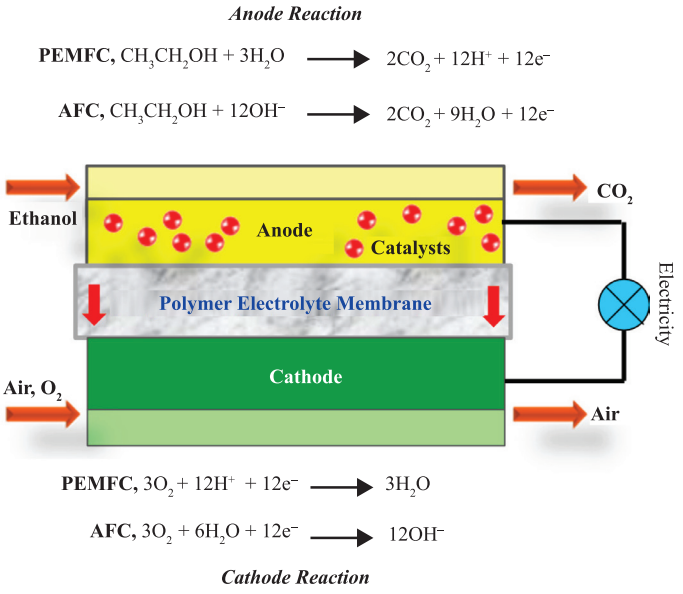

Figure 1: Schematic representation of DEFC in proton-exchange membrane Fuel Cells (PEMFC) and alcohol fuel Cells (AFCs).

Hence, developing effective anode electrocatalysts is imperative to improve the overall reaction rate of the fuel cells. In general, the oxidation of ethanol proceeds via a dual pathway mechanism (Scheme 1).[22] Ethanol can be oxidised to acetaldehyde and subsequently to acetic acid, transferring only four electrons in the process. Ethanol contains two carbons (C2) and during its oxidation reaction (EOR). Various one-carbon (C1) intermediates such as carbon monoxide (CO) and carbohydrate (CH_x), as well as two-carbon (C2) intermediates such as acetaldehyde ($CH_3CH = O$), acetic acid (CH_3COOH), CH_3CO are produced.

Alternatively, the carbon–carbon bond can be cleaved in ethanol or acetaldehyde, yielding the adsorbed single carbon species CO_{ad} and CH_x, ad (with x = 1 in acidic media).[23,24] These species can subsequently be oxidised to CO_2, liberating 12 electrons in total. Strongly adsorbed species such as CO and CH_x could poison the catalyst's surface. Acetic acid marks a 'dead end' in the mechanism, since further oxidation is very difficult. Hence, complete oxidation of ethanol into CO_2 via C–C bond cleavage is mechanistically difficult.[25] Although this is the preferred pathway for a fuel-cell application, the single carbon adsorbates require a high overpotential to be oxidised, and reduce the charge transfer rate of the EOR considerably. In acidic media, currently, the C2 pathway to acetaldehyde and acetic acid with CO_2 formation as a minor contribution, is the main producing pathway for ethanol concentration.[26] Electrochemical analysis, single-crystal model catalyst as well as density functional theory (DFT) calculations suggest that in the current form EOR is produced from partial oxidation of ethanol to acetaldehyde or acetic acid, involving the activation of both the C–H and O–H bonds of ethanol, instead of the C–C bond (Scheme 1).

Cyclic voltammetry (CV): CV is a one type of potentiodynamic electrochemical measurement in which the working electrode potential is ramped linearly versus time and generally used to study the electrochemical properties of an material in solution.

3 Investigation of Electrochemical Properties of Nanomaterials

The development of high-performance and reliable electrochemical energy devices requires a fundamental understanding of the interaction between chemistry and electricity as well as chemical and physical transformations underlying chemical energy storage and conversion applications. A deeper knowledge is required on the fundamental relationships between electrochemical phenomena and materials at nanoscale through interfacial electrochemistry, such as the nature of an electrode–electrolyte interphase, the thermodynamics and kinetics of reactions occurring in the interphase and mass-transport effects throughout it.[27] For example, a particle of ~10 nm contains 10^4–10^5 atoms, 1–5% of which are on the surface of the particle and are important in electrochemical applications such as electrodes.[28,29] The electrode activity is generally estimated by cyclic voltammetry (CV) or linear sweep voltammetry (LSV). In CV, the current is measured, while the voltage is continuously varied (linear sweep). The input parameters are therefore the initial and final voltages and the scan rate, while the output parameters are the voltage values at which the peaks occur and the current intensities. Interestingly, electrochemical measurements have been used for evaluation of the position of energy levels and the band gap of the conducting polymer nanostructures. Electrochemical techniques are also useful for investigating reversibility, stability and rearrangement of the polymer films deposited on the electrode. Voltammetry measurements give information on redox properties, oxidation and reduction potentials. Another technique, electrochemical impedance spectroscopy (EIS), in combination with CV, provides a powerful tool to understand the electrochemical characteristics of electrode materials, including the double-layer capacitance, diffusion impedance, determination of the rate of charge transfer, charge transport

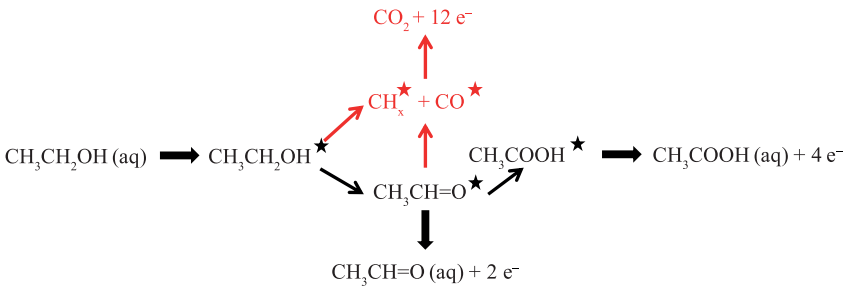

Scheme 1: The reaction pathways involved in the electrooxidation of ethanol to acetaldehyde, acetic acid and CO_2.

processes and solution resistance.[30,31] EIS allows the investigation of charge and mass transport kinetics and charging processes taking place within the analysed material and at the active interfaces of the system. The generalised transmission line circuit model predicts the relevant impedance features of electrode materials in terms of a **Nyquist plot** based on a mathematical approach.[32] The two semi-circles at the highest frequencies, induced by the processes at the metal–support and polymer–solution interfaces, are not always detectable. Often one or even one-half of a semicircle is obtained that partially overlaps with another, depending on the characteristics of the interfacial processes in terms of energy (resistance). Moreover, due to nonhomogeneous separation, surfaces of these semicircles are deformed.[33] Stability can be checked by the Kramers–Kronig transformation and the results can be interpreted as an equivalent circuit (EC) model. Self-made fitting programs can normally be used to construct a quantitative fitting by using the correct electrical circuit; however, the obtained parameters do not have physical equivalents.

Figure 2a represents a typical three-electrode cell for electrochemical measurements of the nanomaterials that were usually deposited on a glassy carbon (GC) as working electrode. This electrode could be changed to a rotating ring-disk electrode to further study the detailed interfacial processes (Figure 2a).

Figure 2b shows the CV of composites of Pd nanoparticles, PEDOT nanospheres (Pd–PEDOT) and graphene (Pd–PEDOT/GE) catalysts coated on GC electrodes. Pd–PEDOT/GE illustrates a pair of well-defined redox peaks with higher peak current indicating the higher electrochemical activity of Pd–PEDOT/GE compared to Pd–PEDOT.[34] Moreover, the peak-to-peak potential separation (ΔE_p) of Pd–PEDOT/GE is 0.09 V, slightly lower than that of Pd–PEDOT (ΔE_p = 0.10 V), signifying the rapid electron transfer between the surface of Pd–PEDOT/GE and the electrolyte.[35] The electrochemically active surface areas (ECSA) of the catalysts can be determined by a calculation of the hydrogen desorption area from cyclic voltammograms (CVs). Importantly, ECSA can provide valuable information on the available active sites of catalysts as well as access a conductive path available to transfer electrons on the electrode surface. Catalysts having higher ECSA value provide an increased active catalytic surface area compared to those with lower ECSA value. Higher number of catalytically active sites is useful for catalysis with current density. Rotating ring-disk electrode voltammetry helps study the electrochemical properties of metal–graphitic hybrid nanostructures (Figure 2c). Pt dispersed on poly-(sodium 4-styrenesulfonate) (PSS)-wrapped SWNTs showed a 50 mV positive shift in the onset potential of ORR compared to a traditional Pt/Carbon black electrode. Additionally, a lower ring current is obtained by the nanotube electrode indicating a higher electron-transfer number per oxygen molecule. Figure 2d shows the impedance plots, which include a semicircle in the range of high frequencies corresponding to electron transfer-limited process, and a linear part in low frequencies representing the diffusion-limited process. Noticeably, the Pd–PEDOT/GE catalyst possesses a smaller high-frequency semicircle diameter, which indicates its smaller charge transfer resistance (R_c, 130 Ω) than that (290 Ω) of Pd–PEDOT suggesting improved electron transfer kinetics and high electrochemical activity of Pd–PEDOT/GE relative to Pd–PEDOT. Further, steady-state currents applied at various voltages have been measured to determine the catalytic activity of a material. The term "onset overpotential" at suitable current density value (0.5–2 mA cm^{-2}) or overpotential at a current density of 10 mA cm^{-2} has been employed to determine the catalytic activity of certain materials. Alternately, the electrochemical active surface area (EASA) of electrodes can be estimated by considering the ratio of the electrochemical double-layer capacitance of the catalytic surface (C_{dl}) and the double-layer capacitance of an atomically smooth planar surface of material per unit area (Cs, specific capacitance) under same electrolyte conditions.[36] Further, C_{dl} can be determined by measuring the non-Faradaic capacitive current related to double-layer charging from the scan rate dependence of the CVs as shown in Figure 3a. The double-layer charging current (i_c) is equal to the product of scan rate (ν) and double-layer capacitance (C_{dl}) as given by;

$$i_c = \upsilon C_{dl} \qquad (13)$$

Hence, a plot of i_c vs ν follows a straight line with a slope equal to C_{dl} as shown in Figure 3(b). The estimated C_{dl} values of graphene oxides (GO) and electrochemically reduced graphene oxides (ErGO) are, respectively, 0.023 and 0.35 mF. Specific capacitance values for carbon electrode materials have been reported in the range of Cs = 0.005–0.055 mF cm^{-2} in alkaline medium, and consider a specific capacitance of Cs = 0.020 mF cm^{-2} for both GO and ErGO as representative values. The estimated EASA values of GO and ErGO are 1.05 cm^2 and

Nyquist plot: A Nyquist plot is a polar plot of the frequency response function of a linear system.

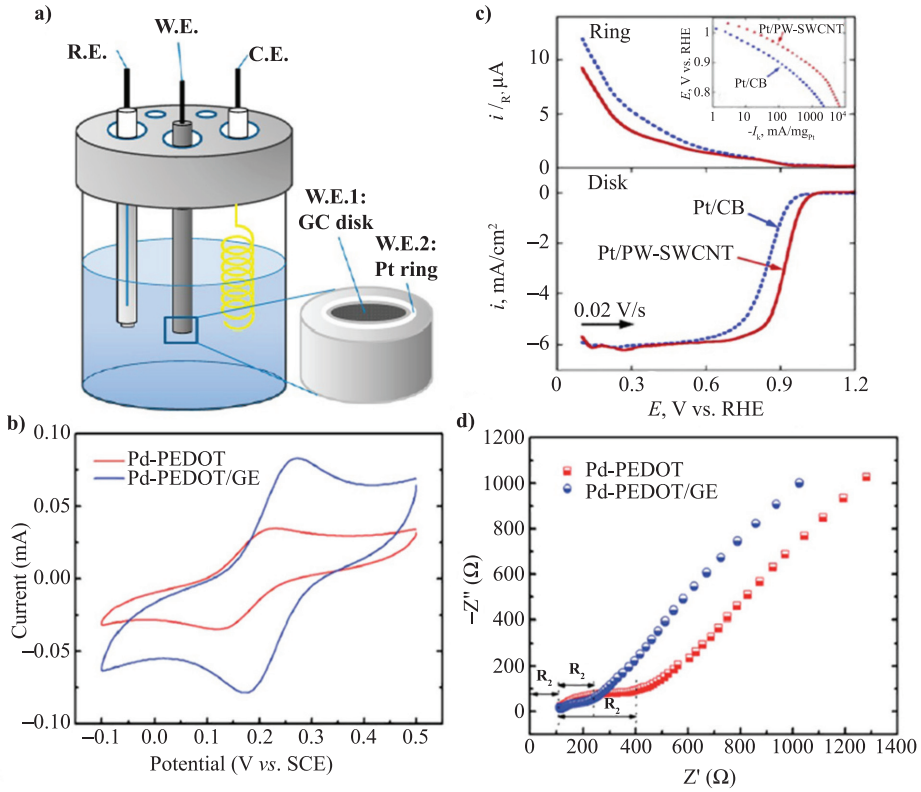

Figure 2: (a) Schematic illustration of a three-electrode cell with a ring-disk electrode. W. E.: working electrode; C. E.: counter electrode; R. E.: reference electrode; GC: glassy carbon. (b) Cyclic voltammograms (CVs) of Pd–PEDOT and Pd–PEDOT/GE catalysts at scan rate: 50 mV s^{-1}), (c) Rotating ring (upper panel) and disk (bottom panel) electrode voltammograms for a Pt-decorated polymer-wrapped single-walled carbon nanotubes (PW-SWCNT, red solid line) and carbon black (CB, blue dot line) for the ORR at 24°C in O_2-saturated 0.1 M $HClO_4$ and the corresponding Tafel plot (inset). Rotating rate = 1600 rpm, E_{Ring} = 1.2 V. and (d) Nyquist plots of Impedance spectroscopy (EIS) at direct current potential: 0.2 V of Pd–PEDOT and Pd–PEDOT/GE catalysts in a 5 mM $[Fe(CN)_6]^{3-/4-}$ mixture (1 : 1) containing 0.1 M KCl solution. J. Phys. Chem. Lett. 2013, 4, 147–160, with the permission of the American Chemical Society. J. Mater. Chem. A, 2015, 3, 1077–1088, with the permission of The Royal Society of Chemistry.

15.9 cm^2. Very recently, Compton et al. reported the direct solution-phase characterisation of individual gold-core silver-shell nanoparticles (NPs) through electrochemical measurements with selectivity achieved between the core and shell components based on their different redox activities.[37] Figure 3c illustrates bright field image of the core–shell formed between the gold core diameter of 1.1 nm and the silver shell thickness of 0.7 nm using high-angle annular dark field scanning transmission electron microscopy (HAADF-STEM) mode. Notably, the electrochemical response of the core–shell NPs was determined where the oxidation of silver can be observed at 0.08 V followed by a broad oxidation attributed to the dissolution of gold and the oxidation of bromide (0.97 V). On the reverse scan, the subsequent reduction of Br_2 occurs at 0.88 V, after the reduction of gold species formed during the forward scan (Figure 3d). Additionally, a quantitative analysis of single bimetallic core–shell NPs was made by conducting a nanoimpact experiment on the basis of potential study. The inset in Figure 3e shows clear spikes in the presence of core–shell NPs when the potential was raised to 0.9 V and larger spikes were observed with further increase in the applied potential to 1.3 V (where the dissolution of the gold NPs is apparent), (Inset: Figure 3e) due to the combined dissolution of both silver shells and gold cores. A potential-dependent study of these processes was then conducted, with the results of 442 impacts (at an average of 63 impacts for each potential studied) presented in Figure 3f. To confirm the quantitative nature of the analysis the average diameter 35.1 ± 0.9 nm of the gold cores was then determined by utilising an 1.9 electron

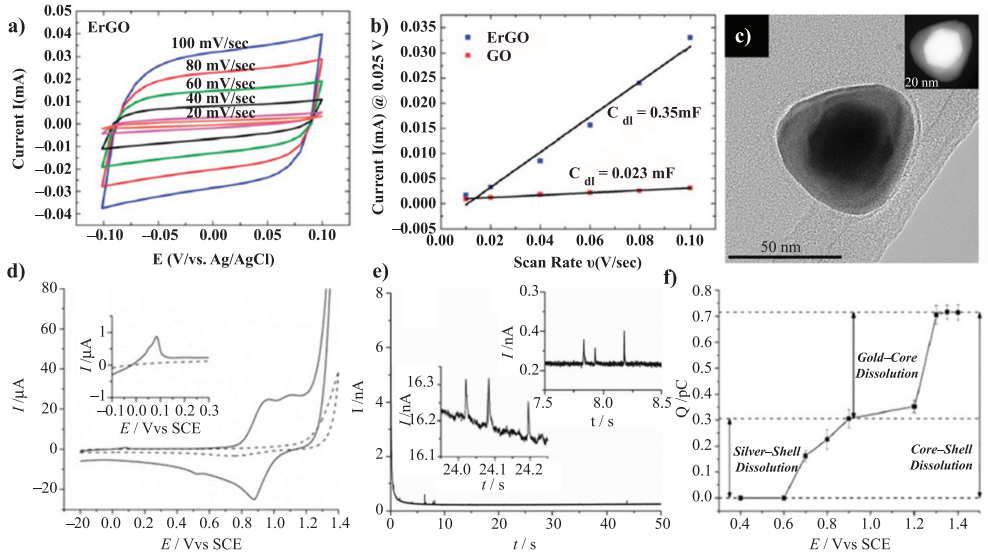

Figure 3: (a) Cyclic voltammograms of ErGO in the potential range of 0.1 V to +0.1 V vs. Ag/AgCl (non-Faradaic region) at scan rates of 100 mV s^{-1}, 80 mV s^{-1}, 60 mV s^{-1}, 40 mV s^{-1}, 20 mV s^{-1} and 10 mV s^{-1} in a N_2-saturated 0.1 M KOH solution. (b) The cathodic charging current measured at 0.025 V vs. Ag/AgCl as a function of scan rate for ErGO and GO. (c) Bright-field TEM image of a gold-core silver-shell nanoparticle along with an HAADF-STEM image (inset). (d) Cyclic voltammograms recorded in 20 mm HCl with a glassy carbon electrode before (dashed line) and after modification with 20 mL of gold-core silver-shell nanoparticles (solid line). (e) Chronoamperograms recorded at a carbon microcylinder electrode at 0.9 V or 1.3 V in a solution of 20 mm HCl with 0.1 pm gold-core silver-shell nanoparticles. (f) The potential dependency of the oxidative impacts of the gold-core silver-shell nanoparticles. Faraday Discuss., 2014, 173, 415–428, with permission of The Royal Society of Chemistry.

oxidation per gold atom. Calculating the thickness of a silver shell on a core of this size, given a charge of 0.3 pC, leads to an average shell thickness of 6.1 ± 0.5 nm.

Then, a Tafel plot can be used to follow the catalytic mechanism of the electrode reaction by following two key parameters, Tafel slop (b) and exchange current density (j_0). For Tafel plot, the overpotential (η) is logarithmically related to current density (j) and the linear portion of the plot is fit to the Tafel equation:[38]

$$\eta = a + b \log j \qquad (14)$$

From the Tafel equation, two important parameters, Tafel slop (b) and exchange current density (j_0) can be determined. The exchange current density is obtained when η is assumed to be zero, and defines the intrinsic catalytic activity of the electrode material under equilibrium conditions. A catalytic material having a high j_0 and a small Tafel slop (b) is highly desirable. Furthermore, the electrocatalytic stability of the catalyst can be established by measuring the current variation with time (i.e., the I–t curve) at high current density for a long period of time as well as by recycling experiment (≥5000 times) by performing CV or LSV.

4 Applications

Nanostructured materials play a critical role in the catalysis of various reactions in fuel cells, resulting in enhanced intrinsic electroactivity with high surface area, superior conductivity and better mass transport. With this electrochemical perspective, nanomaterials have been pursued as both anode and cathode for fuel cells applications. For example, functional nanostructured materials can be used as catalysts or catalyst supports, and as electrodes in energy conversion applications, such as fuel cells. Although fuel cells have made significant impact with their high energy density, and high energy conversion efficiency, the commercialisation of the technology is hampered by high cost, durability and operability problems, which are linked to severe material challenges. Some of its advantages are:

- Novel nanostructured anodic electrocatalysts can minimise the accumulation of strongly adsorbed reaction intermediates to increase EOR kinetics with higher current density, while

Tafel Plot: The Tafel equation is used in electrochemical kinetics relating the rate of an electrochemical reaction to the overpotential.

activating the C–C bond of ethanol to increase EOR efficiency (higher current density from CO_2 formation).
- Precise synthetic approach to synthesise the desired materials with precise controlled composition, size distribution, morphology and heterogeneous nanostructure.
- Advanced characterisation, both *in situ* and *ex situ*, to comprehensively describe the structure of catalysts and the generation of reaction intermediates during EOR using photon (e.g., X-ray), spectroscopic, and imaging techniques.
- The small particle size will aid in a better electrochemical utilisation of the materials.

One of the disadvantages in the synthesis methods employed is the complexity that could increase processing and manufacturing costs, hence there is need to to improve the design aspects in the development of advanced materials for commercialisation. Accomplishments in fuel cell application of electrode materials are summarised in detail here.

4.1 *Fuel cells*

Fuel cells are attractive energy conversion devices, which convert chemical energy directly to electrical energy for portable applications. At the anode, the fuel (e.g., hydrogen) is oxidised to produce protons and electrons. The protons travel across a proton-conducting medium or a polymer electrolyte membrane (PEM), which separate the anode from the cathode in the case of a proton exchange membrane fuel cell useful in transportation and as small portable power source. Direct ethanol or methanol fuel cells (DEFCs or DMFCs) are electrochemical devices that directly convert the chemical energy stored in liquid ethanol or methanol into electricity. Based on the electrolyte used, DAFCs can be divided into two types: acid- and alkaline type. Nanostructured materials played a significant role as catalysts in the development of low-temperature fuel cells ($T < 200$°C), but in current fuel-cell technology, cost, performance and durability issues are big challenges.

Direct Alcohol Fuel Cells (DAFC): An alternative to the polymer electrolyte membrane fuel cell, is the Direct Methanol Fuel Cell (DMFC) or the Direct Ethanol Fuel Cell (DEFC), where alcohol (methanol or ethanol) are used as fuel to the anode.

4.1.1 Noble metals: Electrocatalyst is a key material in fuel cells; however, the catalyst currently used in PEMFCs is based on platinum, which suffers from low activity and poor durability.[39] Noble metals, particularly, platinum-group metals can serve as superior electrocatalysts for ethanol or methanol oxidation reaction and ORR; however, in spite of significant advantages with Pt-based catalysts, high cost limits their large-scale application. Substantial efforts have been made to develop Pt-based catalysts with minimal Pt loading or alternative catalysts based on transition elements via alloying and de-alloying of Pt to synthesise platinum-based core–shell catalysts.[40] Although, in comparison to benchmark Pt catalysts, Pt-alloy electrocatalysts achieve about twice the ORR activity per gram of Pt–group metal, and cost ~35% of equivalent power stacks the long-term stability of the current state-of-the-art catalysts is still not high for most transportation applications.[41] As an alternative to Pt catalysts, Pd-based catalysts have attracted widespread interest owing to their high abundance and greater resistance to CO poisoning.[42] In particular, palladium-based nanostructure is known as an efficient electro-catalyst for ethanol oxidation for fuel-cell applications.[43,44] Importantly, nanostructured materials have well-controlled shape, size and composition, which can rationally modify the electronic and geometric effect of the catalysts, and lead to an improvement in catalytic properties with high activity and stability.[45,46] In earlier reports, Pd nanowires and porous Pd nanoballs connected with three-dimensional Pd nanowires, demonstrated their superior electrocatalytic activity for ethanol oxidation and appear as promising candidates for fuel-cell applications.[47,48] Although various shape- and composition-controlled Pd nanostructures have been widely explored for electrocatalysis, reports on two-dimensional Pd nanostructures are scarce.[49] Ghosh et al.'s work on the electrocatalytic activity of Pd nanoplates (Pd-NPLs) for ethanol oxidation is of special interest.[50] Carbon-based materials support the dispersal of nanostructures to exhibit enhanced electrocatalytic activity to ethanol electrooxidation. A good catalyst support should possess good conductivity and mechanical strength, long-term stability and large specific surface area for loading varied and large number of catalysts into the fuel cells. To overcome the poor utilisation coefficient of aggregated Pd NPs and further enhance the electrocatalytic activity of electrodes, conductive substrates (e.g., carbon) have been selected as supports to disperse the NPs. For instance, highly dispersed Pd NPs on Vulcan XC-72 (VXC), carbon nanotubes (CNT), carbon fibres, and carbon spheres exhibit enhanced electrocatalytic activity towards ethanol electrooxidation.[51,52] An alternative approach is the use of conducting polymers as supporting material having high conductivity. These are currently being

investigated as matrix to incorporate noble metal catalysts for electrooxidation of small molecules such as hydrogen, methanol, formic acid.[49,53,54] Graphene oxides possess high surface area, cost low, have enhanced conductivity, and hence have been chosen as excellent carbon supports for catalysts to achieve enhanced electrochemical performance for a variety of energy applications.[55,56] Ghosh et al. reported the use of reduced RGO nanosheets in combination with nafion as efficient support for metal NPs as they exhibit fascinating catalytic properties.[57] Notably, assembled palladium nanostructures together with prolate ellipsoid-like structures comprising self-assembly of small Pd NPs of 3–4 nm size synthesised in hexagonal mesophases as soft templates are promising electrocatalysts having superior activity and stability for EOR (Figure 4a). Moreover, the introduction of RGO nanosheets along with nafion into the electrode containing Pd nanostructures leads to high electrocatalytic activity and durability for EOR. Figure 4b represents the cyclic voltammogram (CV) of Pd/RGO-Nafion (blue solid line) in pure 1 M NaOH with a characteristic feature of Pd electrodes. Oxygen desorption method is applicable to evaluate the electrochemically active surface area (ECSA) of Pd. The mass-normalised ESCA was calculated for the two electrodes by computing the area under cathodic peaks corresponding to the reaction of Pd oxide monolayers. The calculated data reveals that ECSA of Pd/RGO-Nafion (192 $m^2\ g^{-1}$) is about 4.6 times greater than that of Pd/Nafion (40 $m^2\ g^{-1}$) electrode. This signifies that the Pd/RGO-Nafion-based electrode is more exposed and is available in the solvent environment to undergo the reactions and hence shows increased surface area-induced catalytic effect. Figure 4b illustrates the superposition of the first cyclic voltammogram (black solid line curve) and the 100 cycle (red solid line curve) of Pd/RGO-Nafion run in 1M NaOH containing 1M EtOH at a scan rate of 50 mVs^{-1}.

This voltammetric pattern is represented by two well-defined current peaks, one, the forward peak corresponds to ethanol oxidation activity, and the other, the reverse potential scan, formed prior to Pd-O blocking, corresponds to oxidation of both freshly adsorbed ethanol and adsorbed carbonaceous species. The peak current and the onset potential of the Faradaic current (E_{onset}) on the forward scan indicate the electrocatalytic activity of the catalyst for EOR. The main quantitative parameters measured from these two voltammograms have been tabulated (Table 1). During the potential cycles, the E_{onset} shifts to a more negative potential from –534 mV at the 1st cycle to –590 mV after 100 cycles underscoring the enhancement in the kinetics of ethanol oxidation. The influence of high surface area of RGO as support (Table 1) clearly highlights that RGO-Nafion support exhibited higher current density. The electrochemical performance of assembled Pd nanostructure and Pd-based nanostructures under comparable reaction conditions are listed in Table 1. Interestingly, the superiority of Pd/RGO-Nafion in terms of current density (7166 $mA{\cdot}cm^{-2}{\cdot}mg^{-1}$) is obvious, being nearly 4.4 times higher than that of previously reported Pd nanowires (1327 $mA{\cdot}cm^{-2}{\cdot}mg^{-1}$) synthesised in hexagonal mesophases (Table 1).

Faradaic current: The net current generated by the reduction or oxidation of chemical substance at an working electrode.

Table 1: Comparison of electrochemical performance of Pd nanostructured electrocatalysts for ethanol oxidation.

Electrode	E_{onset}, mV/SCE	E_f, mV/SCE	E_b, mV/SCE	I_f, $mA.cm^{-2}$	I_f, $mA.cm^{-2}.mg^{-1}$ of Pd	Reference
Pd/Nafion	–590	–185	–382	8.55	1745	57
Pd/RGO-Nafion	–622	–186	–312	14.22	5925	57
Commercial Pd black catalyst	–550	~ –200	~ –301	0.65	–	106
Tetrahedral Pd nanocrystal	–590	–219	~ –305	3.83	–	106
Pd/Nf-graphene	–600	–	–	0.56		107
C-Pd Nanoballs/Nafion	–550	–151	–296	–	–	48
Pd nanowires/Nafion	–664	–166	–278	–	1327	47
CNT-Pd/Nafion	–564	–242	–451	–	364	52
CNT-Pd/Nafion	–670	–245	–332	–	3540	52
C-Pd	–680	–209	~ –310	–	63	108
C-Pd	–579	–219	~ –360	–	42	109
C-Pd	–619	–203	~ –330	–	85	109

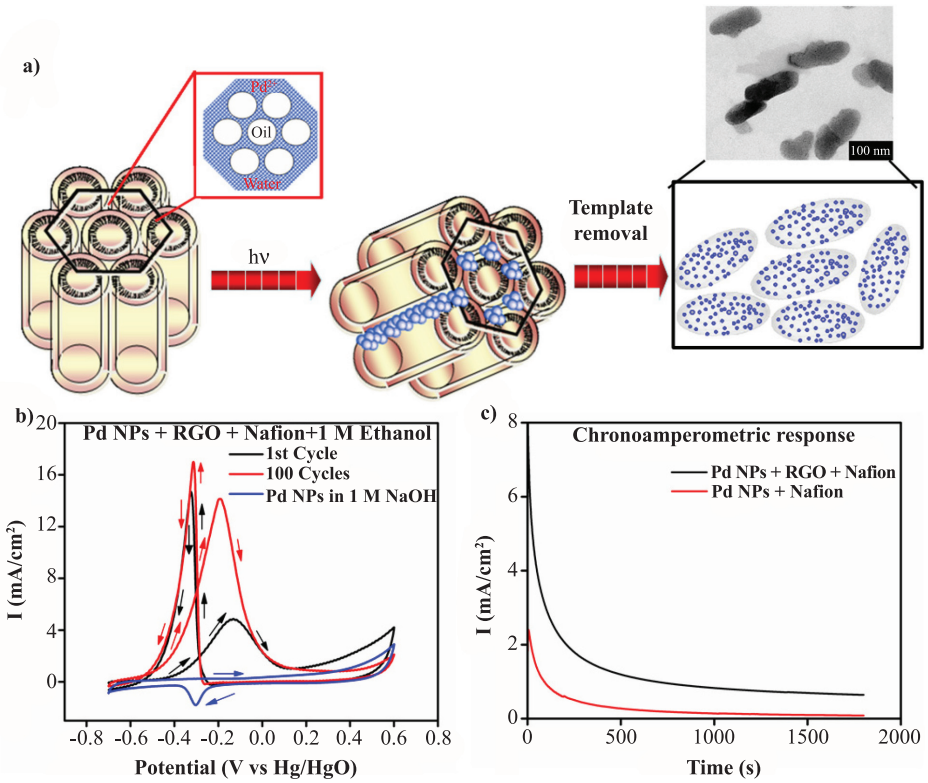

Figure 4: (a) Schematic representation of light-induced synthesis of Pd nanostructures in hexagonal mesophases. Inset: Transmission electron micrographs of Pd nanostructures synthesised in hexagonal mesophases by 12 h UV-irradiation. (b) Cyclic voltammograms of Pd NPs/RGO-Nafion in 1 M NaOH (blue solid line) superposition of the first (black solid line curve) and the 100th (red solid line curve) cyclic voltammetric runs associated with the electrocatalytic oxidation of 1 M EtOH in 1 M NaOH. The working electrode was a glassy carbon disk modified with the Pd nanostructures. The reference electrode was an Hg/HgO (1 M KOH) electrode. The scan rate was 50 mVs^{-1}. (c) Chronoamperometric curves for the ethanol electrooxidation at –0.30 V vs Hg/HgO on a glassy carbon electrode modified with Pd/Nafion (black curve) and Pd/RGO-Nafion (red curve). Inset: the comparison of chronoamperometric response of Pd/Nafion and Pd/RGO-Nafion at normalised current (I). J. Mater. Chem. A 2015, 3, 9517–9527, with the permission of The Royal Society of Chemistry.

The catalyst stability as a function of time is also important for its practical application in fuel cells. The stability of catalytic performance was then investigated by chronoamperometric (CA) measurements, where current density-time (I *vs* t) curves at constant potentials were recorded (Figure 4c). In the first several minutes, both catalysts exhibited a pronounced current decay owing to the accumulation of poisonous intermediates. The current density decayed in the first 500s and attained a steady state thereafter indicating that these Pd NPs form very stable film on glassy carbon electrode surface and Pd/RGO-Nafion catalyst exhibited the highest limiting as well as the initial current showing the highest activity than the Pd/Nafion catalysts. Further, Ghosh et al. also showed that, in comparison to their bulk counterparts, CP nanostructure-supported catalytic materials display improved electrode activity in ethanol oxidation which can be useful in direct ethanol fuel cells (DFFCs). The poly(diphenylbutadyine) (PDPB) polymer nanofibre can be used as support with high the catalytic activity of Pd nanoplates for oxidation of ethanol. The nanofibre morphology of poly(diphenylbutadyine) polymer helps in the effective dispersion of Pd nanoplates facilitating easier access of ethanol to the catalytic sites. The dispersion of Pd nanoplates with polymer nanofibres is connected with catalytic response to a higher activity. These results show that the polymer-supported Pd nanoplate catalyst is a promising anode catalyst in DAFCs. A deep understanding of the influence of various experimental parameters and polymer support on catalytic properties and mechanism will eventually lead to a rational design of advanced catalysts with substantially

enhanced performance. A series of Pt NP-based electrocatalysts supported on conducting polymer has been used for the electrocatalytic oxidation of methanol.

4.1.2 Transition metal oxides: Although Pt-based metals or alloys are regarded as robust and efficient catalysts for oxidation and reduction reactions, their high cost and limited availability necessitate the exploitation of new non-precious metal catalysts.[58] The development of an active material via a naturally abundant and economically viable method has remained elusive in energy conversion applications. In fact, ORR is a challenging reaction due to slower kinetics and stability of the cathode catalyst material under cycling in acidic or alkaline conditions during operation. However, one critical issue to be addressed is the lack of effective electrocatalysts for the four-electron ($4e^-$) reduction of O_2 (ORR) at a relatively low overpotential.[59] Accordingly, non-precious transition metal oxides and, in particular manganese oxides (MnO_x), are regarded as alternative ORR catalysts with reasonable catalytic activity, low cost and structural stability for primary alkaline-based fuel cells.[60] Suib et al. reported a manganese oxide (MnO_2) catalyst having dual nature (OER and ORR catalysis), a potential alternative for high-cost Pt and its alloys, iridium, and ruthenium oxide catalysts.[61,62] Srabanti et al. reported of porous manganese oxide (Mn_2O_3) nanoballs (NBs) as bifunctional electrocatalysts for oxygen reduction and evolution reaction.[63] A facile and large-scale synthesis of thermally stable, crystalline, pure and copper-doped Mn_2O_3 NBs was achieved by a microwave-assisted hydrothermal method. Pure and doped Mn_2O_3 NBs can be effectively used as electrode materials with electrocatalytic activity toward the 4-electron oxygen reduction reaction. Figure 5a-c illustrates the formation of porous nanoball Cu^{+2}-doped Mn_2O_3 formed by the self-assembly of very small NPs as evident from FESEM. The average diameter of the Cu-Mn_2O_3 NBs was found to be 800 nm. The elemental distribution of the material was further characterised by energy-dispersive spectroscopic (EDS) mapping. The EDS elemental mapping clearly confirmed the presence and distribution of Mn, O, and Cu elements in Cu-Mn_2O_3 NBs as shown in Figure 5c-f. To evaluate the electrochemical activity of ORR of pure and doped Mn_2O_3, rotating disk electrode (RDE) experiments were performed. Pt wire and Ag/AgCl (Sat. KCl) were used as counter and reference electrodes, respectively, and 0.1 M KOH was used as an electrolyte. High-purity O_2 gas was purged for 30 min before each RDE experiment to get the electrolyte saturated with O_2. RDE measurements were further carried out to reveal the ORR kinetics of the as-prepared catalysts. The RDE polarisation curves of Cu-Mn_2O_3 NBs with increase in rotation rate lead to the enhancement of current density of ~5.8 $mAcm^{-2}$ (Figure 5g). Koutecky-Levich plot follows parallel straight lines for different potentials in mixed kinetic diffusion-controlled region indicating the number of electrons transferred per O_2 molecule and the active surface area for the reaction do not change significantly within the potential range studied (Figure 5h). From the analysis of the Koutecky-Levich plot, the value of n was found to be in the range of 3.4–3.9 (Figure 5i).[64, 65] Copper doping in Mn_2O_3, NBs reveals its enormous impact on the electrocatalytic activity with a high current density for ORR, which is supported by 5.2 times higher electrochemically active surface area (EASA) in comparison with pure Mn_2O_3. The ORR current values obtained for both Mn_2O_3 and Cu-Mn_2O_3 NBs were highly stable over 10,000s of continuous operation at a constant potential of −0.4 V in chronoamperometry measurement, demonstrating their use as effective electrocatalysts for alkaline fuel cells. Hence, the microwave-assisted approach provides a general platform for fabricating well-defined porous metal oxide nanostructures with prospective application as low-cost catalysts for alkaline fuel cells. Recently, mixed metal oxides displaying excellent catalytic activity have been investigated as one of the most promising candidates for ORR in an alkaline medium. Maiyalagan et al. described the excellent electrocatalytic activity of lithium cobalt oxide-based spinels as synergistic bifunctional catalysts for OER and ORR,[66] and Muhler et al. of cobalt–manganese-based spinels as synergistic bifunctional catalysts.[67]

4.1.3 Carbon-based catalysts: Carbonaceous materials are considered as one of the most inexpensive catalyst alternatives to benchmark Pt catalysts as C is widely abundant and durable, as well as less expensive than Pt. They can be utilised as catalyst supports or as metal-free catalysts with superior physicochemical properties such as large surface areas and high electrical conductivity, which make them suitable in electrocatalysis of oxygen.[68–71] Yang et al. reported that sandwich-like graphene-based carbon nitride nanosheets serve as metal-free electrocatalysts for ORR with excellent performance in combination with an enhanced electrical conductivity.[72] Seredych et al. developed a novel ORR catalyst using polyHIPE

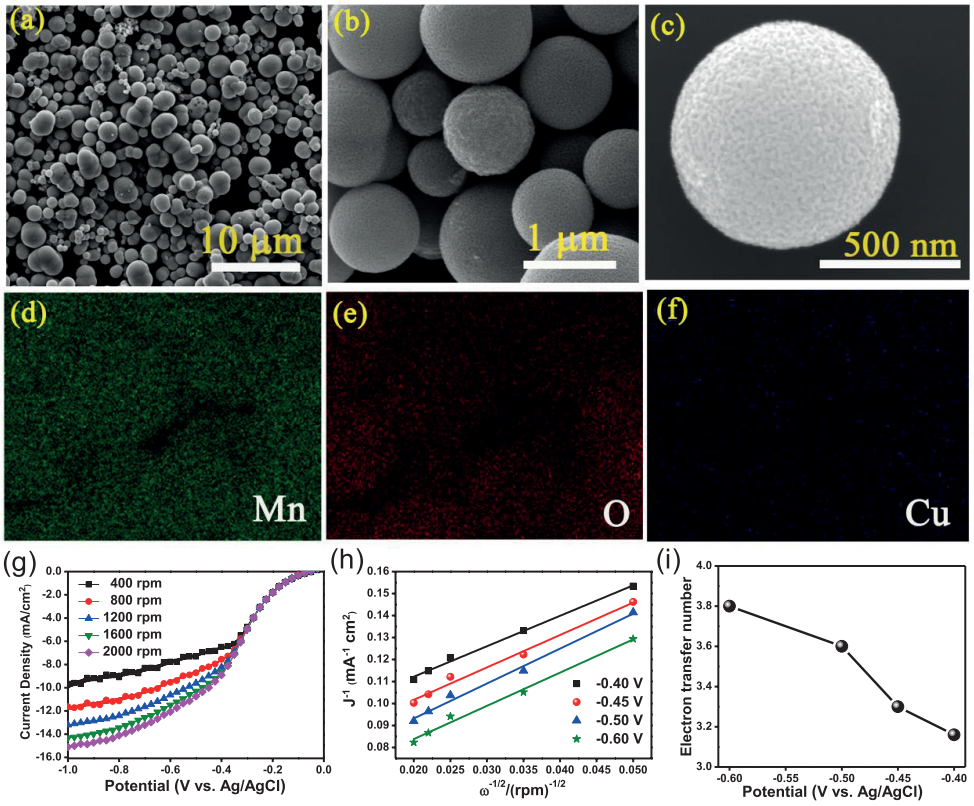

Figure 5: a-c) SEM images with different magnification, (d) Mn, (e) O, (f) Cu elemental mapping of Cu-doped Mn_2O_3 nanoballs and catalytic activity of copper-doped Mn_2O_3 nanoballs for oxygen reduction reaction (ORR), (g) Rotating disk voltammograms of Cu-Mn_2O_3 in O_2-saturated 0.1 M KOH at different rotation rates for oxygen reduction, (h) the corresponding Koutecky–Levich plots (J^{-1} vs. $\omega^{-0.5}$) at different potentials of Cu-Mn_2O_3 NBs, (i) the electron transfer number (n) profiles obtained from Koutecky–Levich plots. Catalysis Sci. Technol. 2016, 6, 1417–1429, with the permission of The Royal Society of Chemistry, UK.

(polymerised high internal phase emulsion)-based carbon derived from co-reacted furfuryl alcohol and tannin.[73] The polyHIPE carbons show high electrochemical stability and better tolerance to methanol than Pt/C. The presence of a very high volume of ultramicropores and the highest degree of defects on the surface create high kinetic current density. Xu et al. reported micron-sized commercial polyacrylonitrile-based carbon fibre (PAN-CF) electrode modified by using an electrochemical method, converting its inherent pyridinic-N into 2-pyridone (or 2-hydroxyl pyridine) functional group existing in the three-dimensional active layers with remarkable ORR catalytic activity and stability.[74] A series of studies has shown that carbon nanomaterials (carbon nanotubes, grapheme, etc) doped with heteroatom (such as S, P and N) could be an efficient, low-cost, metal-free alternative to Pt for ORR.[75–77] Yu et al. for the first time have developed a simple plasma-etching technology to produce metal-free nitrogen-doped single-walled carbon nanotube catalysts with good electrocatalytic activity and long-term stability towards ORR in acidic medium.[78] Choi et al. reported a series of binary and ternary dopings of nitrogen, boron, and phosphorus into carbon for enhancing electrochemical oxygen reduction activity with remarkable performance enhancements. Charge delocalisation of the carbon atoms or number of edge sites of the carbon is a significant factor in deciding the catalytic activity in carbon-based catalysts.[79] Zhan et al. developed mesoporous carbon foam co-doped with nitrogen and phosphorus that has a large surface area (1,663 m^2 g^{-1}) and good electrocatalytic properties for ORR (Figure 6a-e). This material was fabricated using a scalable, one-step process involving the pyrolysis of a polyaniline aerogel synthesised in the presence of phytic acid.[80] The linear scan voltammogram (LSV) curves illustrate the electrocatalytic performance of NPMC-1000 with a positive onset potential of 0.94 V *vs* reversible hydrogen electrode (RHE) and a half-wave potential of 0.85 V versus RHE, which

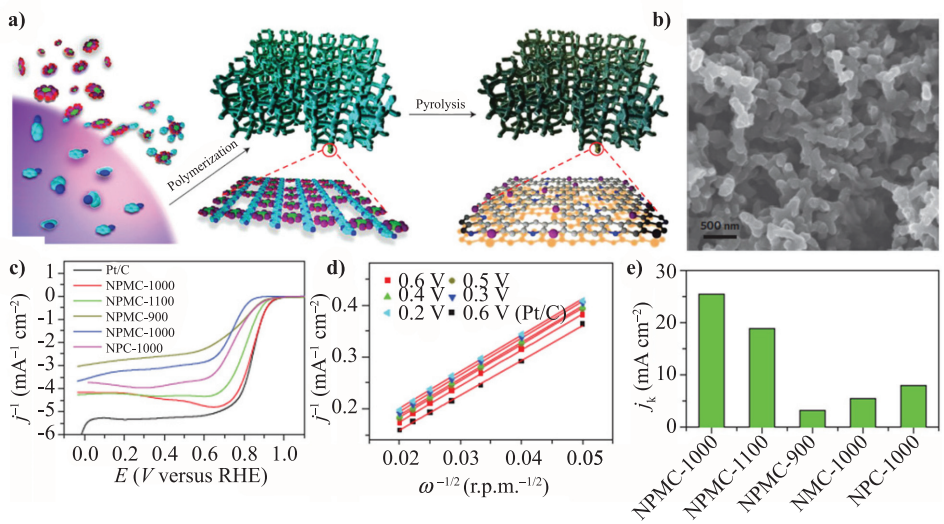

Figure 6: (a) Preparation of the N and P co-doped porous carbon (NPMC) electrocatalysts. (a) Schematic illustration of the preparation process for the NPMC foams. (b) SEM image of PANi aerogel. (c) Electrocatalytic activity for ORR, linear scan voltammogram (LSV) curves for NPMC-900, NPMC-1000, NPMC-1100, NMC-1000, NPC-1000 and commercial Pt/C catalyst at an RDE (1600 rpm) in O_2-saturated 0.1 M KOH solution. Scan rate, 5 mV s^{-1}. (d) K–L plots for NPMC-1000 and Pt/C at various potentials. (e) Kinetic current of various samples for O_2 reduction at 0.65 V. Nature Nanotechnology, 2015, 10, 444–452, with the permission of The Nature Publishers.

are comparable to those of Pt/C (Figure 6c). The K–L plots show linear relationship between kinetic current and ω, the electrode rotating rate, with a similar slope for the NPMC-1000 and Pt/C electrodes, from which n was determined to be ~4.0, suggesting a four-electron pathway for ORR (Figure 6d). The kinetic current calculated from the intercept of the linearly fitted K–L plots at 0.65 V (*vs* RHE) for the NPMC-1000 electrode is the largest among all the metal-free catalysts investigated in this study (Figure 6e).

Stevenson et al. discussed the mechanism of the oxygen reduction reaction (ORR) at undoped and nitrogen-doped carbon nanotubes (CNTs and N-CNTs) in neutral and alkaline aqueous solutions through a "pseudo"-four-electron pathway involving a catalytic regenerative process. In this process, hydroperoxide is chemically disproportionated to form hydroxide (OH^-) and molecular oxygen (O_2) with over 1000-fold enhancement at rates comparable to the best known peroxide decomposition catalysts.[81] Wood et al. summarise the recent progress on nitrogen/carbon structures designed for energy application and improvements in well-established fabrication/modification processes.[82] Chen et al. studied the effect of the structure, composition of carbon precursors and oxygen reduction reaction performance of nitrogen-doped carbon materials.[83] In an another interesting example, Ferrero et al. discovered high-surface area N-doped mesoporous carbon capsules with iron traces exhibiting outstanding electrocatalytic activity in oxygen reduction reaction in both alkaline and acidic media with remarkable performance stability (3500 cycles between 0.6 and 1.0 V *vs* RHE).[84] However, the dopant concentration in present carbon-based catalysts is low (N, 4–6 at%, B, 0–2.24 at%, and 1–2 at% of S), which limits the improvement of the catalytic activity of carbon-based catalysts.

4.1.4 Hybrid catalysts: Hybrid nanostructures assembled by metal/metal oxides and combined with electronically conductive agents, for example, carbon nanotubes, carbon nanofibres, conducting polymers, reduced graphene oxide (rGO) sheets have attracted a considerable attention.[85,86,50] Specifically, graphene sheets have aroused great promise because of their excellent electrical conductivity, high surface area (calculated value = 2630 m^2 g^{-1}) and chemical stability.[87,57] Hence, graphene functionalised metal oxide hybrid as electrode material can combine the catalytic activity of metal with high surface area of carbon support by preventing the aggregation of catalysts, and possesses good electrical conductivity to facilitate electronic transfer, offering easy access of the electrolyte to the electrode surface, allowing increased utilisation of active material and

enhanced stability. A significant effort has been devoted to create hybrid materials that contain a carbon layer as well as an inorganic layer.[88–91] The hybrid shows excellent electrocatalytic activities and kinetics for ORR which compares favourably with those of the Pt/C catalyst, together with superior durability, a four-electron pathway and excellent methanol tolerance.[92,93] The dual-active-site mechanism originating from synergic effects between each component is responsible for the excellent performance of the hybrid material. This development offers an attractive catalyst material for large-scale fuel-cell and water-splitting technologies. Xiao et al. report of the morphologically controlled synthesis of Co_3O_4 nanorods (NR), nanocubes (NC) and nano-octahedrons (OC) with different exposed nanocrystalline surfaces ({110}, {100}, and {111}) uniformly anchored on graphene sheets as highly efficient ORR catalysts.[94] The Co_3O_4 nanocrystal/RGO hybrid nanostructure-based electrodes were interrogated by cyclic voltammetry (Figure 7a). The Co_3O_4 NP (size, 10 nm) on the surface of RGO sheets exhibited very poor ORR activity with an onset potential of ~ –0.25 V vs. Hg/HgO, whereas Co_3O_4 NR/RGO hybrids showed a much more positive ORR onset potential (~ –0.1 V) suggesting higher ORR catalytic activity than Co_3O_4 NP/RGO. Notably, the Co_3O_4 NC/RGO with six exposed {100} surfaces and Co_3O_4 OC/RGO nanocomposites with eight exposed {111} surfaces achieved even more positive onset potentials, for example, ~ –0.06 V for Co_3O_4 NC/RGO, and ~ –0.04 V for Co_3O_4 OC/RGO, closely approaching that of Pt/C, the gold standard for ORR catalysts. As can be seen from the LSV curves in Figure 7b, among the four Co_3O_4/RGO composite electrodes, the Co_3O_4 NP/RGO composite catalyst shows the lowest onset potential, whereas the Co_3O_4 OC/RGO composite shows the highest one.

The ORR catalytic activity of the Co_3O_4/RGO hybrid catalysts can also be gleaned from the Tafel slopes at low and high overpotentials (Figure 7c). The E vs log (–J) curves of the samples similarly show two Tafel slopes at low and high overpotentials, respectively, indicating a similar change in reaction mechanisms with the potential. As can be observed from Figure 7c, the Co_3O_4 NC (83.7 mV/decade) and Co_3O_4 OC (101.4 mV/decade) on RGO sheets exhibit smaller Tafel slopes at the over-potentials from 20.05 V to 20.10 V than the Co_3O_4 NR/RGO hybrid (115.6 mV/decade) in 0.1 M KOH electrolyte demonstrating high ORR catalytic activities close to that of the commercial Pt/C catalyst (93.9 mV/decade). To examine possible crossover effect for catalytic performance, the electrocatalytic selectivity of the Co_3O_4/RGO composite electrode against electro-oxidation of methanol molecules has been

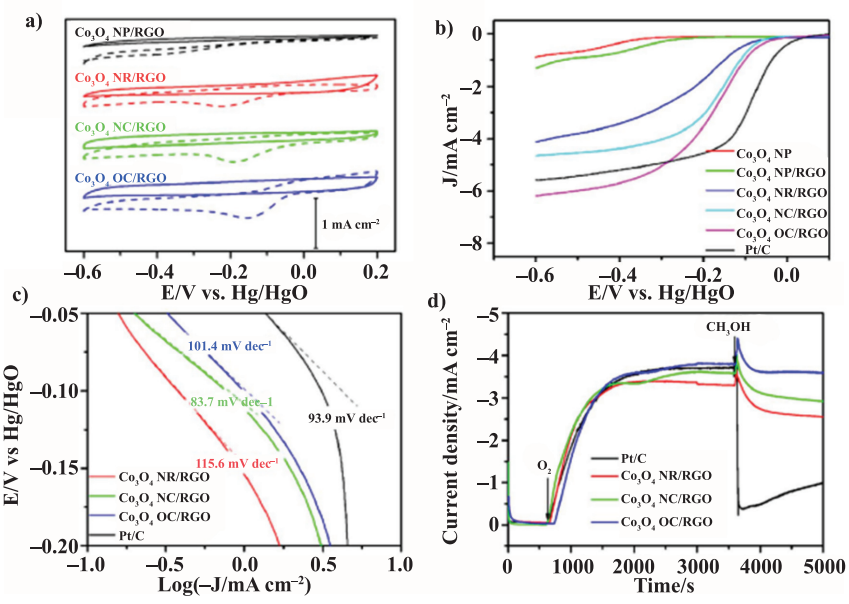

Figure 7: (a) CV curves of Co_3O_4 nanocrystals/RGO composites on glassy carbon electrodes in N_2-saturated (solid line) or O_2-saturated 0.1 MKOH (dash line), (b) Rotating-disk voltammograms, (c) Tafel plots for the Co_3O_4/RGO composite electrodes and the commercial Pt/C electrode, and (d) J-T chronoamperometric responses at 20.40 V vs Hg/HgO reference electrode at a rotating rate of 2400 rpm. The 0.1 M KOH solution electrolyte is firstly bubbled by N_2 for 30 min, and then is introduced by O_2 gas for around 3000 s, and is finally added by 20 vol% of methanol. Scientific Reports, 2013, 3, 2300 with the permission of The Nature Publishers.

measured (Figure 7d). Tian et al. demonstrated the bi-functional catalytic activity of a nitrogen-doped graphene/carbon nanotube hybrid for tailor-made catalytic applications.[95] Guo et al. synthesised FePt nanoparticles assembled on graphene as highly stable catalyst for oxygen reduction reaction, which showed nearly no activity change after 10,000 potential sweeps.[96] Shen et al. further reported the synthesis of novel Pt electrocatalyst encapsulated inside nitrogen-doped carbon nanocages (Pt@NCNC), which presents excellent alcohol-tolerant ORR activity and durability in acidic media, far superior to the Pt counterpart immobilised outside the nanocages (Pt/NCNC).[97] Li et al. reported a simple and cost-effective strategy to fabricate nitrogen and phosphorus dual-doped graphene/carbon nanosheets (N,P-GCNS) with N, P-doped carbon sandwiching few-layer-thick graphene shows outstanding catalytic activity toward ORR, which is attributed to the synergistic effects between doped N and P atoms, full exposure of the active sites on the surface of the N,P-GCNS nanosheets, high conductivity of the incorporated graphene, and large surface area and hierarchical pores for sufficient contact and rapid transportation of the reactants.[98]

5 Mechanistic Understanding

It is crucial to gain an understanding of the reaction mechanism of the catalytic reaction on the catalyst surface to improve the performance of catalysts. Liang et al. proposed ethanol oxidation through dissociative adsorption of ethanol, which proceeds rather quickly and the rate-determining step was the removal of the adsorbed ethoxi by the adsorbed hydroxyl on the Pd electrode using cyclic voltammetry technique.[99] In the potential range smaller than −0.5 V vs Hg/HgO, the oxidation of the absorbed and adsorbed hydrogen occurs on Pd electrode:[100]

$$\mathrm{Pd-(H)_{abs/ads}+OH^- \leftrightarrow Pd+H_2O+e^-.} \quad (15)$$

According to the literature, in the potential range above −150 mV, palladium (II) oxide forms a layer on the surface of the catalyst.[101] Although its mechanism is as yet unclear, it is widely accepted that OH^- ions are first chemisorbed at the initial stage of the oxide formation. The oxidation reaction may be rationalised by the following mechanism:[101]

$$\mathrm{Pd+OH^- \leftrightarrow Pd-(OH)_{ads}+e^-} \quad (16)$$

$$\mathrm{Pd-(OH)_{ads}+OH^- \leftrightarrow Pd-O+H_2O+e^-} \quad (17)$$

$$\mathrm{Pd-(OH)_{ads}+Pd-(OH)_{ads} \leftrightarrow Pd-(O)+H_2O.} \quad (18)$$

The sharp peak on the reverse sweep is attributed to the reduction of the Pd(II) oxide, according to:

$$\mathrm{Pd-(O)+H_2O+2e^- \leftrightarrow Pd+2OH^-} \quad (19)$$

After the addition of ethanol, the signal corresponding to oxidation and reduction of palladium disappeared leading to the apparition of two peaks related to the ethanol oxidation process. The forward scan peak is related to the oxidation of freshly chemisorbed species issued from alcohol adsorption (equation 20 and 21), while the reverse scan peak represents the removal of carbonaceous species not completely oxidised in the forward scan and the reactivation of the Pd-NPLs surface with the reduction of the Pd oxide (equation 19).[102]

$$\mathrm{Pd+CH_3CH_2OH \leftrightarrow Pd-(CH_3CH_2OH)_{ads}} \quad (20)$$

$$\mathrm{Pd-(CH_3CH_2OH)_{ads}+3OH^- \rightarrow Pd-(CH_3CO)_{ads}+3H_2O+3e^-} \quad (21)$$

On the other hand, oxygen can be directly reduced to water with the concomitant consumption of four electrons per O_2 molecule (equation 4). Alternatively, oxygen can be reduced indirectly, forming H_2O_2 as an intermediate and only two electrons per O_2 molecule are consumed (equation 5). In the presence of catalysts, the first step involves electron transfer from electrode surface and one layer of salvation shell to solvated O_2, which involves many elementary steps.

$$\mathrm{M-OH+\left[O_2.(H_2O)_n\right]_{aq}+e^- \rightarrow M-OH+\left[O_2^-(H_2O)_n\right]_{aq}} \quad (22)$$

$$\mathrm{\left[O_2^-(H_2O)_n\right]_{aq} \rightarrow \left(O_2^-\right)_{ads}+nH_2O} \quad (23)$$

$$\mathrm{\left(O_2^-\right)_{ads}+nH_2O \rightarrow \left(HO_2^-\right)_{ads}+OH^-} \quad (24)$$

Initially, electron transfer to $O_{2,aq}$ enables the formation of $(O_2^{\bullet -})_{aq}$, which then undergoes desolvation and subsequent adsorption on the oxide substructure of the Pt surface to form $(O_2^{\bullet -})_{ads}$, followed by proton transfer to form

adsorbed hydroperoxyl radical, $(HO_2^{\bullet})_{ads}$. Then, electron transfer to $(HO_2^{\bullet})_{ads}$ yields $(HO_2^{\bullet-})_{ads}$. The binding energy of $(HO_2^{\bullet-})_{ads}$ on the oxide substructure of Pt is likely to be lower than that on the oxide-free Pt site, which leads to the facile desorption of HO_2^- anion into the electrolyte. The interaction between the $O_2^{\bullet}(H_2O)_n$ cluster and the surface hydroxyl species provides certain nonspecificity to the identity of the underlying electrode metal. This can be overcome by using non-noble metals and their oxides as electrode materials for ORR in alkaline media.

The identity of the active site of a catalyst is blocked by the progress in the development of advanced electrocatalysts. Consequently, theoretical analysis and experimental methods provide an understanding of electrocatalysis at the atomic level as well as a fundamental insight into designing improved electrocatalysts. Chai et al. proposed active sites and mechanisms for oxygen reduction reaction on nitrogen-doped carbon alloy catalysts by the first-principles molecular dynamics simulations, and second the reaction of Gibbs free energy for each electrochemical elementary step.[103] Notably, a particular structure of a nitrogen pair-doped Stone–Wales defect provides a good active site and its catalytic activity can be tuned by the curvature around the active site at the maximum limiting potential (0.80 V) in the volcano plot for the ORR activity of carbon catalysts. Additionally, various advanced tools, for example, high-resolution X-ray crystal structure analysis, extended X-ray absorption fine structure (EXAFS), and electron paramagnetic resonance (EPR) have been utilised to correlate the electronic structure with the activity of electrocatalysts. For example, Wood et al. provided in-depth analysis of functional groups present at the surface of ion-implanted vulcan and graphitic vulcan through the use of X-ray photoelectron spectroscopy (XPS) and near-edge X-ray adsorption fine structure spectroscopy (NEXAFS) suggesting superior catalytic activity of nitrogen-doped carbon-supported catalyst architectures originated from improved numbers of nucleation sites, an increase in electrochemical stability compared with standard carbon, greatly improved conductivity to facilitate charge transport and enhanced catalyst-support interactions, which prevent precious metal agglomeration due to migration/coalescence and dissolution/reprecipitation across the carbon surface.[102] It is widely accepted that conducting ORR on Pt in alkaline media is disadvantageous not only from the perspective of cost as well as from a kinetics point of view due to significant peroxide generation at typical operating potential of fuel cells. Ramaswamy et al. proposed that the presence of adsorbed hydroxyl species on Pt catalyst sites during ORR not only inhibits direct molecular adsorption of O_2 but also promotes a $2e^-$ reduction of O_2 to HO_2^- by an outer-sphere electron transfer mechanism.[104] Moreover, the formation of oxide species on the metal surface and its interaction with the solvated molecular O_2 cause a nonspecific outer-sphere mechanism, which promotes only the two-electron reduction process. On the other hand, to improve the Faradaic efficiency of the ORR, the electrocatalytic inner-sphere electron transfer mechanism is important for facilitation of direct adsorption of molecular oxygen and the stabilisation of the peroxide intermediate on the active site are emphasised with the usage of chalcogen-based transition metals. Lim et al. investigated the mechanisms of oxygen reduction reaction on defective graphene-supported Pt_{13} nanoparticles with density functional theory (DFT) predictions using projector-augmented wave (PAW) method within the generalised gradient approximation (GGA).[105] Interestingly, the defective graphene support may provide a balance in the binding of ORR intermediates on Pt_{13} NPs by tuning the relatively high reactivity of free Pt_{13} NPs that bind the ORR intermediates too strongly, which subsequently will lead to slow kinetics for O_2 dissociation from 0.37 to 0.16 eV, as well as the energy barrier of the rate-limiting step by reducing the stability of the HO^* species. It has been determined that an activation-free energy (0.16 eV) for O_2 dissociation from adsorbed O_2^* at a bridge site on the supported Pt_{13} NP into $O^* + O^*$ species is lower than the free energy barrier (0.29 eV) for the formation of HOO^* species from adsorbed O_2^*, which suggests a preference for direct pathway as the initial step in the ORR mechanism.

6 Summary

As rapid development of nanostructured materials continues, this review shows the impact of catalytic materials on alternative energy devices, based on the electrochemical processes of nanomaterials, fundamental aspects of electron and mass transfer at the surface during catalysis and an understanding of the activity and stability of electrocatalysts. Electrochemistry addresses the chemical and physical transformations underlying chemical energy storage and conversion and their relationship to limitations in the performance of electrochemical systems. The interrelationship between interfacial electrochemistry and nanoscience gives rise to new possibilities for designing chemical surfaces by controlling the structures at the molecular level, leading to innovative metal or semiconductor

surfaces and charge transfer lengths. Functional nanostructures facilitate excellent mobility, solubility, morphology tunability and the possibility to tailor the surface properties, which can follow through electrochemical characterisation. Hybrid structures have shown real efficiency gains in terms of energy density and stability. Advanced techniques enable comprehensive characterisation of the electrochemical interface for successful application of electrocatalysts. The surface science in combination with electrochemical approaches has opened up opportunity to control the surface structure and composition, which are useful parameters in the field of electrocatalysis. It is important to develop environment-friendly, highly efficient and selective catalysts with low loading of material to make cost-effective catalysts for large-scale industrial applications.

Acknowledgements

The authors thank the Director, CSIR-CGCRI, for kind permission to publish the work. One of the authors (SG) is thankful to the Council of Scientific & Industrial Research (CSIR), India, for providing CSIR-Senior Research Associate (Scientists' Pool Scheme) award.

Received 14 August 2016.

References

1. A.S. Arico, P. Bruce, B. Scrosati, J.M. Tarascon and W. van Schalkwijk, Nanostructured materials for advanced energy conversion and storage devices. *Nat. Mater.* **4**, 366–377 (2005).
2. Q. Zhang, E. Uchaker, S.L. Candelaria and G. Cao, Nanomaterials for energy conversion and storage. *Chem. Soc. Rev.* **42**, 3127–3171 (2013).
3. E.R. Leite (Ed), Nanostructured Materials Electrochemical Energy Production and Storage, Chapter 3, "Electrochemistry, Nanomaterials, and Nanostructures", P. Ro. Bueno and C. Gabrielli, ISBN: 978-0-387-49322-0, Springer, (2009) pp. 81–150.
4. S. Ghosh, M. Thandavarayan and R.N. Basu, Nanostructured conducting polymers for energy applications: towards a sustainable platform. *Nanoscale* **8**, 6921–6947 (2016).
5. H. Abe and K. Ariga, *Mater. Today* **19**, 12–18 (2016).
6. J.O.M. Bockris and A.K.N. Reddy, Modern Electrochemistry. Vol. 1. 1973, New York: A Plenum/ Rosetta Edition.
7. D.M. Adams, L. Brus, C.E.D. Chidsey, S. Creager, C. Creutz, C.R. Kagan, P.V. Kamat, M. Lieberman, S. Lindsay, R.A. Marcus, R.M. Metzger, M.E. Michel-Beyerle, J.R. Miller, M.D. Newton, D.R. Rolison, O. Sankey, K.S. Schanze, J. Yardley and X.Y. Zhu, Charge transfer on the nanoscale: Current status. *J. Phys. Chem. B* **107**, 6668–6697 (2003).
8. J.W. Schultze, A. Heidelberg, C. Rosenkranz, T. Schapers and G. Staikov, Principles of electrochemical nanotechnology and their application for materials and systems. *Electrochim. Acta* **51**, 775–786 (2005).
9. Y. Holade, A. Lehoux, H. Remita, K.B. Kokoh and T.W. Napporn, Au@Pt Core–Shell Mesoporous Nanoballs and Nanoparticles as Efficient Electrocatalysts toward Formic Acid and Glucose Oxidation. *J. Phys. Chem. C.* **119**, 27529–27539 (2015).
10. S. Ghosh, Y. Holade, H. Remita, K. Servat, P. Beaunier, A. Hagège, K. Boniface Kokoh and T.W. Napporn, One-pot synthesis of reduced graphene oxide supported gold-based nanomaterials as robust nanocatalysts for glucose electrooxidation. *Electrochim. Acta* **212**, 864–875(2016).
11. Y. Holade, C. Morais, K. Servat, T.W. Napporn and K.B. Kokoh, Toward the electrochemical valorization of glycerol: Fourier transform infrared spectroscopic and chromatographic studies. *ACS Catal.* **3**, 2403–2411 (2013).
12. J.H. Wee, Applications of proton exchange membrane fuel cell systems. *Renewable and Sustainable Energy Rev.* **11**, 1720–1738 (2007).
13. S.P.S. Badwal, S. Giddey, A. Kulkarni, J. Goel and S. Basu, Direct ethanol fuel cells for transport and stationary applications—A comprehensive review. *Appl. Energy* **145,** 80–103 (2015).
14. M. Carmo, D.L. Fritz, J. Mergel, and D. Stolten, A comprehensive review on PEM water electrolysis. *Int. J. Hydrogen Energy* **38**, 4901–4934 (2013).
15. A.J. Bard and L.R. Faulkner, Electrochemical Methods: Fundamentals and Applications. 2nd ed, John Wiley & Sons, Inc. (2001).
16. S. Trasatti, Physical electrochemistry of ceramic oxides. *Electrochim. Acta* **36**, 225–241 (1991).
17. D. Chen, C. Chen, Z.M. Baiyee, Z. Shao and F. Ciucci, Nonstoichiometric Oxides as Low-Cost and Highly-Efficient Oxygen Reduction/Evolution Catalysts for Low-Temperature Electrochemical Devices. *Chem. Rev.* **115**, 9869–9921 (2015).
18. W. Vielstich, A. Lamm and H.A. Gasteiger, Handbook of Fuel Cells—Fundamentals, Technology and Applications, Wiley, Chichester, 2003.
19. K. Kinoshita, Electrochemical Oxygen Technology, Wiley, New York, (1992).
20. U.A. Paulus, T.J. Schmidt, H.A. Gasteiger and R.J. Behm, Oxygen Reduction on a High-Surface Area Pt/Vulcan Carbon Catalyst: A Thin-Film Rotating Ring-Disk Study. *J. Electroanal. Chem.* **495**, 134–145 (2001).
21. A.T. Haug and R.E. White, Oxygen Diffusion Coefficient and Solubility in a New Proton Exchange Membrane. *J. Electrochem. Soc.* **147**, 980–983 (2000).
22. S.C.S. Lai and M.T.M. Koper, Electro-oxidation of ethanol and acetaldehyde on platinum single-crystal electrodes. *Faraday Discuss.* **140**, 399–416 (2008).
23. G.A. Camara and T. Iwasita, Parallel pathways of ethanol oxidation: The effect of ethanol concentration. *J. Electroanal. Chem.*, **578**, 315–321(2005).

24. J. Shin, W.J. Tornquist, C. Korzeniewski and C.S. Hoaglund, Elementary steps in the oxidation and dissociative chemisorption of ethanol on smooth and stepped surface planes of platinum electrodes. *Surf. Sci.* **364**, 122–130 (1996).
25. A. Wieckowski, J. Sobrowski, P. Zelenay and K. Franaszczuk, Adsorption of acetic acid on platinum, gold and rhodium electrodes. *Electrochim. Acta*. **26**, 1111–1119 (1981).
26. H. Wang, Z. Jusys and R.J. Behm, Ethanol Electrooxidation on a Carbon-Supported Pt Catalyst: Reaction Kinetics and Product Yields. *J. Phys. Chem. B*. **108**, 19413–19424 (2004).
27. W. Plieth, Electrochemistry for Materials Science, 1st Ed, Elsevier, (2007).
28. T. Basché, A. Bottin, C. Li, K. Müllen, J.-H. Kim, B.-H. Sohn, P. Prabhakaran, K.-S. Lee, Energy and Charge Transfer in Nanoscale Hybrid Materials, *Macromol. Rapid Commun*. **36**, 1026–1046 (2015).
29. J.W. Schultze, A. Heidelberg, C. Rosenkranz, T. Schapers, and G. Staikov, Principles of electrochemical nanotechnology and their application for materials and systems. *Electrochim. Acta* **51**, 775–786 (2005).
30. E. Barsoukov and J.R. Macdonald, Impedance Spectroscopy: Theory, Experiment, and Applications, Wiley Interscience, Hoboken, NJ, (2005).
31. M.D. Levi, Y. Gofer, D. Aurbach and A. Berlin, EIS evidence for charge trapping in n-doped poly-3-(3,4,5-trifluorophenyl) thiophene. *Electrochim. Acta*. **49**, 433–444 (2004).
32. B.W. Johnson, D.C. Read, P. Christensen, A. Mamnet and R.D. Armstrong, Impedance characteristics of conducting polythiophene films. *J. Electroanal. Chem*. **364**, 103–109 (1994).
33. J.R. Macdonald, Impedance spectroscopy: old problems and new developments. *Electrochim. Acta* **35**, 1483–1492 (1990).
34. R. Yue, H. Wang, D. Bin, J. Xu, Y. Du, W. Lu and J. Guo, Facile one-pot synthesis of Pd–PEDOT/graphene nanocomposites with hierarchical structure and high electrocatalytic performance for ethanol oxidation. *J. Mater. Chem. A* **3**, 1077–1088 (2015).
35. L. Tang, Y. Wang, Y. Li, H. Feng, J. Lu and J. Li, *Adv. Funct. Mater.* **19,** 2782–2789 (2009).
36. S.K. Bikkarolla, P. Cumpson, P. Joseph and P. Papakonstantinou, Oxygen reduction reaction by electrochemically reduced grapheme oxide. *Faraday Discuss* **173**, 415–428 (2014).
37. L.R. Holt, B.J. Plowman, N.P. Young, K. Tschulik and R.G. Compton, The Electrochemical Characterization of Single Core–Shell Nanoparticles. *Angew. Chem. Int*. **55**, 397–400 (2016).
38. T. Shinagawa, A.T. Garcia-Esparza and K. Takanabe, Insight on Tafel slopes from a microkinetic analysis of aqueous electrocatalysis for energy conversion. *Sci. Reports* **5**, 13801 (2015).
39. X. Wang, S.-Il Choi, L.T. Roling, M. Luo, C. Ma, L. Zhang, M. Chi, J. Liu, Z. Xie, J.A. Herron, M. Mavrikakis and Y. Xia, Palladium–platinum core-shell icosahedra with substantially enhanced activity and durability towards oxygen reduction. *Nat. Commun*. **6**, 7594 (2015).
40. C. Wang, N.M. Markovic and V.R. Stamenkovic, Advanced Platinum Alloy Electrocatalysts for the Oxygen Reduction Reaction. *ACS Catal*. **2**, 891–898 (2012).
41. M.K. Debe, Electrocatalyst approaches and challenges for automotive fuel cells. *Nature* **486**, 43–51 (2012).
42. C. Bianchini and P.K. Shen, Palladium-Based Electrocatalysts for Alcohol Oxidation in Half Cells and in Direct Alcohol Fuel Cells. *Chem. Rev*. **109,** 4183–206 (2009).
43. X. Huang, Y. Li, Y. Li, H. Zhou, X. Duan and Y. Huang, *Nano Lett*. **12**, 4265–4270 (2012).
44. P.S. Roy and S.K. Bhattacharya, Size-controlled synthesis and characterization of polyvinyl alcohol-coated platinum nanoparticles: role of particle size and capping polymer on the electrocatalytic activity. *Catal. Sci. Technol*. **3**, 1314–1323 (2013).
45. F. Ksar, L. Ramos, B. Keita, L. Nadjo, P. Beaunier and H. Remita, Bimetallic Palladium–Gold Nanostructures: Application in Ethanol Oxidation. *Chem. Mater*. **21**, 3677–3683 (2009).
46. C. Koenigsmann, A.C. Santulli, E. Sutter and S.S. Wong, Ambient Surfactantless Synthesis, Growth Mechanism, and Size-Dependent Electrocatalytic Behavior of High-Quality, Single Crystalline Palladium Nanowires. *ACS Nano* **5**, 7471–7487 (2011).
47. F. Ksar, G. Surendran, L. Ramos, B. Keita, L. Nadjo, E. Prouzet, P. Beaunier, A. Hagège, F. Audonnet and H. Remita, Palladium Nanowires Synthesized in Hexagonal Mesophases: Application in Ethanol Electrooxidation. *Chem. Mater.* **21**, 1612–1617 (2009).
48. G. Surendran, F. Ksar, L. Ramos, B. Keita, L. Nadjo, E. Prouzet, P. Beaunier, P. Dieudonné, F. Audonnet and H. Remita, Palladium Nanoballs Synthesized in Hexagonal Mesophases. *J. Phys. Chem. C* **112**, 10740–10744 (2008).
49. X. Huang, S. Tang, X. Mu, Y. Dai, G. Chen, Z. Zhou, F. Ruan, Z. Yang and N. Zheng, Freestanding palladium nanosheets with plasmonic and catalytic properties. *Nat. Nano*. **6**, 28–32 (2011).
50. S. Ghosh, A.L. Teillout, D. Floresyona, P.d. Oliveira, A. Hagège and H. Remita, Conducting polymer-supported palladium nanoplates for applications in direct alcohol oxidation. *Int. J. Hydrogen Energy*. **40**, 4951–4959 (2015).
51. J. Zhang, Y. Mo, M.B. Vukmirovic, R. Klie, K. Sasaki and R.R. Adzic, Platinum Monolayer Electrocatalysts for O_2 Reduction: Pt Monolayer on Pd(111) and on Carbon-Supported Pd Nanoparticles. *J. Phys. Chem. B*. **108**, 10955–10964 (2004).
52. N. Mackiewicz, G. Surendran, H. Remita, B. Keita, G. Zhang, L. Nadjo, A. Hagège, E. Doris and C. Mioskowski, Supramolecular Self-Assembly of Amphiphiles on Carbon Nanotubes: A Versatile Strategy for the Construction of CNT/Metal Nanohybrids, Application to Electrocatalysis. *J. Am. Chem. Soc*.**130**, 8110–8111 (2008).

53. P. Xu, X. Han, B. Zhang, Y. Du and H.L. Wang, Multifunctional polymer–metal nanocomposites via direct chemical reduction by conjugated polymers. *Chem. Soc. Rev*. **43**, 1349–1360 (2014).
54. S. Ghosh, K.A. Natalie, L. Ramos, S. Remita, A. Dazzi, A.D. Besseau, F. Goubard, P.H. Aubert and H. Remita, Conducting polymer nanostructures for photocatalysis under visible light. *Nat. Mater*. **14**, 505–511 (2015).
55. Y. Li, H. Wang, L. Xie, Y. Liang, G. Hong and H. Dai, MoS_2 Nanoparticles Grown on Graphene: An Advanced Catalyst for the Hydrogen Evolution Reaction. *J. Am. Chem. Soc*. **133**, 7296–7299 (2011).
56. Y. Liang, Y. Li, H. Wang, J. Zhou, J. Wang, T. Regier and H. Dai, Co_3O_4 nanocrystals on graphene as a synergistic catalyst for oxygen reduction reaction. *Nat. Mater*. **10**, 780–786 (2011).
57. S. Ghosh, H. Remita, P. Kar, S. Choudhury, S. Sardar, P. Beaunier, P.S. Roy, S.K. Bhattacharya and S.K. Pal, Facile synthesis of Pd nanostructures in hexagonal mesophases as a promising electrocatalyst for ethanol oxidation. *J. Mater. Chem. A* **3**, 9517–9527 (2015).
58. N. Jung, D.Y. Chung, J. Ryu, S.J. Yoo and Y.E. Sung, Pt Based Nanoarchitecture and Catalyst Design for Fuel Cell Applications. *Nano Today* **9**, 433–456 (2014).
59. Y. Li, W. Zhou, H. Wang, L. Xie, Y. Liang, F. Wei, J.C. Idrobo, S.J. Pennycook and H. Dai, An Oxygen Reduction Electrocatalyst Based on Carbon Nanotube-Graphene Complexes. *Nat. Nanotechnol*. **7**, 394–400 (2012).
60. X. Deng and H. Tüysüz, Cobalt-Oxide-Based Materials as Water Oxidation Catalyst: Recent Progress and Challenges. *ACS Catal*. **4**, 3701–3714 (2014).
61. Y. Gorlin and T.F. Jaramillo, A Bifunctional Nonprecious Metal Catalyst for Oxygen Reduction and Water Oxidation. *J. Am. Chem. Soc*. **132**, 13612–13614 (2010).
62. Y. Meng, W. Song, H. Huang, Z. Ren, S.Y. Chen and S.L. Suib, Structure–Property Relationship of Bifunctional MnO_2 Nanostructures: Highly Efficient, Ultra-Stable Electrochemical Water Oxidation and Oxygen Reduction Reaction Catalysts Identified in Alkaline Media. *J. Am. Chem. Soc*. **136**, 11452–11464 (2014).
63. S. Ghosh, P. Kar, N. Bhandary, S. Basu, S. Sardar, D. Majumdar, S.K. Bhattacharya, A. Bhaumik, P. Lemmens and S.K. Pal, Microwave-assisted synthesis of porous Mn_2O_3 nanoballs as bifunctional electrocatalyst for oxygen reduction and evolution reaction. *Catal. Sci. Technol*. **6**, 1417–1429 (2016).
64. R.C. Weastled, Handbook of Chemistry and physics, 55th Ed: R.C. West, Cleveland, OH, CRC Press, (1984).
65. J. Zhang, (Ed.) PEM Fuel Cell Electrocatalysts and Catalyst Layers C. Song, J. Zhang, chapter 2, Electrocatalytic Oxygen Reduction Reaction, Springer, (2008).
66. T. Maiyalagan, K.A. Jarvis, S. Therese, P.J. Ferreira and A. Manthiram, Spinel-Type Lithium Cobalt Oxide as a Bifunctional Electrocatalyst for the Oxygen Evolution and Oxygen Reduction Reactions. *Nat. Commun*. **5**, 3949–3956 (2014).
67. A. Zhao, J. Masa, W. Xia, A. Maljusch, M.G. Willinger, G. Clavel, K. Xie, R. Schlögl, W. Schuhmann and M. Muhler, Spinel Mn–Co Oxide in N-Doped Carbon Nanotubes as a Bifunctional Electrocatalyst Synthesized by Oxidative Cutting. *J. Am. Chem. Soc*. **136**, 7551–7554 (2014).
68. K. Gong, F. Du, Z. Xia, M. Durstock and L. Dai, Nitrogen-Doped Carbon Nanotube Arrays with High Electrocatalytic Activity for Oxygen Reduction. *Science*. **323**, 760–764 (2009).
69. Y. Zhao, R. Nakamura, K. Kamiya, S. Nakanishi and K. Hashimoto, Nitrogen-doped carbon nanomaterials as non-metal electrocatalysts for water oxidation. *Nat. Commun*. **4**, 2390 (2013).
70. J. Liu, S. Zhao, C. Li, M. Yang, Y. Yang, Y. Liu, Y. Lifshitz, S.T. Lee and Z. Kang, Carbon Nanodot Surface Modifications Initiate Highly Efficient, Stable Catalysts for Both Oxygen Evolution and Reduction Reactions. *Adv. Energy Mater*. **6**, (2016), DOI: 10.1002/aenm.201502039.
71. M. Shao, Q. Chang, J.P. Dodelet, and R. Chenitz, Recent Advances in Electrocatalysts for Oxygen Reduction Reaction. *Chem. Rev*. **116**, 3594–3657 (2016).
72. S. Yang, X. Feng, X. Wang, and K. Müllen, Graphene-based carbon nitride nanosheets as efficient metal-free electrocatalysts for oxygen reduction reactions. *Angew. Chem. Chem. Int. Ed.* **50**, 5339–5343 (2011).
73. M. Seredych, A. Szczurek, V. Fierro, A. Celzard, and T.J. Bandosz, Electrochemical Reduction of Oxygen on Hydrophobic Ultramicroporous PolyHIPE Carbon. *ACS Catal.* **6**, 5618–5628 (2016).
74. H. Xu, G. Xia, H. Liu, S. Xia and Y. Lu, Electrochemical activation of commercial polyacrylonitrile-based carbon fiber for the oxygen reduction reaction. *Phys. Chem. Chem. Phys*. **17**, 7707–7713 (2015).
75. E. Cruz-Silva, F. López-Urías, E. Muñoz-Sandoval, B.G. Sumpter, H. Terrones, J.-C. Charlier, V. Meunier and M. Terrones, Electronic transport and mechanical properties of phosphorus- and phosphorus-nitrogen-doped carbon nanotubes. *ACS Nano* **3**, 1913–1921 (2009).
76. L. Yang, S. Jiang, Y. Zhao, L. Zhu, S. Chen, X. Wang, Q. Wu, J. Ma, Y. Ma, Z. Hu, Boron-doped carbon nanotubes as metal-free electrocatalysts for the oxygen reduction reaction. *Angew. Chem. Chem. Int. Ed.* **50**, 7132–7135 (2011).
77. Z. Yang, Z. Yao, G. Li, G. Fang, H. Nie, Z. Liu, X. Zhou, X. Chen, and S. Huang, Sulfur-doped graphene as an efficient metal-free cathode catalyst for oxygen reduction. *ACS Nano*. **6**, 205–211 (2011).
78. D. Yu, Q. Zhang and L.J. Dai, Highly efficient metal-free growth of nitrogen-doped single-walled carbon nanotubes on plasma-etched substrates for oxygen reduction. *Am. Chem. Soc*. **132**, 15127–15129 (2010).
79. C.H. Choi, S.H. Park and S.I. Woo, Binary and ternary doping of nitrogen, boron, and phosphorus into carbon for enhancing electrochemical oxygen reduction activity. *ACS Nano* **6**, 7084–7091 (2012).

80. J. Zhang, Z. Zhao, Z. Xia and L. Dai, A metal-free bifunctional electrocatalyst for oxygen reduction and oxygen evolution reactions. *Nat. Nanotechnol.* **10**, 444–452 (2015).
81. J.D.W. Camacho and K.J. Stevenson, Mechanistic Discussion of the Oxygen Reduction Reaction at Nitrogen-Doped Carbon Nanotubes. *J. Phys. Chem. C* **115**, 20002–20010 (2011).
82. K.N. Wood, R.O. Hayrea and S. Pylypenko, Recent progress on nitrogen/carbon structures designed for use in energy and sustainability applications. *Energy Environ. Sci*. **7**, 1212–1249 (2014).
83. L. Chen, Z. Chen, Z. Huang, Z. Huang, Y. Wang, H. Li, H. Zhou and Y. Kuang, Influence of Carbon Precursors on the Structure, Composition, and Oxygen Reduction Reaction Performance of Nitrogen-Doped Carbon Materials. *J. Phys. Chem. C* **119**, 28757–28765 (2015).
84. G.A. Ferrero, K. Preuss, A. Marinovic, A.B. Jorge, N. Mansor, D.J.L. Brett, A.B. Fuertes, M. Sevilla and M.M. Titirici, Fe–N-Doped Carbon Capsules with Outstanding Electrochemical Performance and Stability for the Oxygen Reduction Reaction in Both Acid and Alkaline Conditions. *ACS Nano* **10**, 5922–5932 (2016).
85. O.S. Kwon, T. Kim, J.S. Lee, S.J. Park, H.W. Park, M. Kang, J.E. Lee, J. Jang and H. Yoon, Fabrication of Graphene Sheets Intercalated with Manganese Oxide/Carbon Nanofibers: Toward High-Capacity Energy Storage. *Small* **9**, 248–254 (2013).
86. D. Yu, K. Goh, H. Wang, L. Wei, W. Jiang, Q. Zhang, L. Dai and Y. Chen, Scalable synthesis of hierarchically structured carbon nanotube–graphene fibres for capacitive energy storage. *Nat. Nanotech.* **9**, 555–562 (2014).
87. M.F. El-Kady, V. Strong, S. Dubin and R.B. Kaner, Laser scribing of high-performance and flexible graphene-based electrochemical capacitors. *Science* **335**, 1326–1330 (2012).
88. G.L. Tian, M.Q. Zhao, D. Yu, X.Y. Kong, J.Q. Huang, Q. Zhang and F. Wei, Nitrogen-Doped Graphene/Carbon Nanotube Hybrids: In Situ Formation on Bifunctional Catalysts and Their Superior Electrocatalytic Activity for Oxygen Evolution/Reduction Reaction. *Small* **10**, 2251–2259 (2014).
89. Y. Hou, Z. Wen, S. Cui, S. Ci, S. Mao and J.H. Chen, An Advanced Nitrogen-Doped Graphene/Cobalt-Embedded Porous Carbon Polyhedron Hybrid for Efficient Catalysis of Oxygen Reduction and Water Splitting. *Adv. Funct. Mater*. **25**, 872–882 (2015).
90. J.E. Kim, J. Lim, G.Y. Lee, S.H. Choi, U.N. Maiti, W.J. Lee, H.J. Lee, and S.O. Kim, Cobalt-Embedded Nitrogen Doped Carbon Nanotubes: A Bifunctional Catalyst for Oxygen Electrode Reactions in a Wide pH Range. *ACS Appl. Mater. Interfaces* **8**, 1571–1577 (2016).
91. X. Li, Y. Fang, X. Lin, M. Tian, X. An, Y. Fu, R. Li, J. Jin and J. Ma, MOF derived Co_3O_4 nanoparticles embedded in N-doped mesoporous carbon layer/MWCNT hybrids: extraordinary bi-functional electrocatalysts for OER and ORR.*J. Mater. Chem. A*. **3**, 17392–17402 (2015).
92. H.W. Park, D.U. Lee, M.G. Park, R. Ahmed, M.H. Seo, L.F. Nazar and Z. Chen, Perovskite–Nitrogen-Doped Carbon Nanotube Composite as Bifunctional Catalysts for Rechargeable Lithium–Air Batteries. *ChemSusChem*. **8**, 1058–1065 (2015).
93. D.U. Lee, H.W. Park, M.G. Park, V. Ismayilov and Z. Chen, Synergistic Bifunctional Catalyst Design based on Perovskite Oxide Nanoparticles and Intertwined Carbon Nanotubes for Rechargeable Zinc–Air Battery Applications. *ACS Appl. Mater. Interfaces* **7**, 902–910 (2015).
94. J. Xiao, Q. Kuang, S. Yang, F. Xiao, S. Wang and L. Guo, Surface Structure Dependent Electrocatalytic Activity of Co_3O_4 Anchored on Graphene Sheets toward Oxygen Reduction Reaction. *Sci Reports*. **3**, 2300 (2013).
95. G.L. Tian, M.Q. Zhao, D. Yu, X.Y. Kong, J.Q. Huang, Q. Zhang and F. Wei, Nitrogen-Doped Graphene/Carbon Nanotube Hybrids: In Situ Formation on Bifunctional Catalysts and Their Superior Electrocatalytic Activity for Oxygen Evolution/Reduction Reaction. *Small*. **10**, 2251–2259 (2014).
96. S. Guo and S. Sun, FePt nanoparticles assembled on graphene as enhanced catalyst for oxygen reduction reaction. *J. Am. Chem. Soc.* **134**, 2492–2495 (2012).
97. L. Shen, T. Sun, O. Zhuo, R. Che, D. Li, Y. Ji, Y. Bu, Q. Wu, L. Yang, Q. Chen, X. Wang, and Z. Hu, Alcohol-Tolerant Platinum Electrocatalyst for Oxygen Reduction by Encapsulating Platinum Nanoparticles inside Nitrogen-Doped Carbon Nanocages. *ACS Appl. Materials Interfaces* **8**, 16664–16669 (2016).
98. R. Li, Z. Wei and X. Gou, Nitrogen and Phosphorus Dual-Doped Graphene/Carbon Nanosheets as Bifunctional Electrocatalysts for Oxygen Reduction and Evolution. *ACS Catal*. **5**, 4133–4142 (2015).
99. Z.X. Liang, T.S. Zhao, J.B. Xu and L.D. Zhu, Mechanism study of the ethanol oxidation reaction on palladium in alkaline media. *Electrochim. Acta* **54**, 2203–2208 (2009).
100. M. Grdeń, M. Łukaszewski, G. Jerkiewicz and A. Czerwiński, Electrochemical behaviour of palladium electrode: Oxidation, electrodissolution and ionic adsorption. *Electrochim. Acta* **53**, 7583–98 (2008).
101. J. Prabhuram, R. Manoharan and H.N. Vasan, Effects of incorporation of Cu and Ag in Pd on electrochemical oxidation of methanol in alkaline solution. *J. Appl. Electrochem.* **28**, 935–41 (1998).
102. L. Chai, Z. Hou, D.J. Shu, T. Ikeda and K. Terakura, Active Sites and Mechanisms for Oxygen Reduction Reaction on Nitrogen-Doped Carbon Alloy Catalysts: Stone–Wales Defect and Curvature Effect. *J. Am. Chem. Soc.* **136**, 13629–13640 (2014).
103. K.N. Wood, S.T. Christensen, D. Nordlund, A.A. Dameron, C. Ngo, H. Dinh, T. Gennett, R. O'Hayre and S. Pylypenko, Spectroscopic investigation of nitrogen functionalized carbon materials. *Surf. Interface Anal*. **48**, 283–292 (2016).

104. N. Ramaswamy and S. Mukerjee, Influence of Inner- and Outer-Sphere Electron Transfer Mechanisms during Electrocatalysis of Oxygen Reduction in Alkaline Media. *J. Phys. Chem. C* **115**, 18015–18026 (2011).
105. D.H. Lim and J. Wilcox, Mechanisms of the Oxygen Reduction Reaction on Defective Graphene-Supported Pt Nanoparticles from First-Principles. *J. Phys. Chem. C* **116**, 3653–3660 (2012).
106. N. Tian, Z.-Y. Zhou, N.-F. Yu, L.-Y. Wang and S.-G. Sun, Direct Electrodeposition of Tetrahexahedral Pd Nanocrystals with High-Index Facets and High Catalytic Activity for Ethanol Electrooxidation. *J. Am. Chem. Soc.* **132**, 7580–7581 (2010).
107. S. Yang, J. Dong, Z. Yao, C. Shen, X. Shi, Y. Tian, S. Lin and X. Zhang, One-Pot Synthesis of Graphene-Supported Monodisperse Pd Nanoparticles as Catalyst for Formic Acid Electro-oxidation. *Sci. Reports* **4**, 4501 (2014).
108. M. Grdeń, M. Łukaszewski, G. Jerkiewicz and A. Czerwiński, Electrochemical behaviour of palladium electrode: Oxidation, electrodissolution and ionic adsorption. *Electrochem. Acta* **53**, 7583–7598 (2008).
109. C. Xu, P.k. Shen and Y. Liu, Ethanol electrooxidation on Pt/C and Pd/C catalysts promoted with oxide. *J. Power Sources* **164**, 527–531 (2007).

Srabanti Ghosh received her PhD degree in Chemistry from UGC-DAE Consortium for Scientific Research, Kolkata Centre, and Jadavpur University, India. She is presently working as a CSIR-SRA (Scientists' Pool Scheme) in Fuel Cell & Battery Division, Central Glass and Ceramic Research Institute, Kolkata, India. Her research interests include synthesis, characterization and application of quantum dots, dendrimer nanocomposites and conducting polymers. Her current research work is focused on energy application of conducting polymer nanostructures, low cost catalysts for solar light harvesting and fuel cell applications. She received MRSI Young Scientists Award in Young Scientists Colloquium organized by Material Research Society of India (MRSI), and Young Investigator Award in Gordon Radiation Chemistry (GRC), New Hampshire, USA. She has been awarded Postdoctoral Fellowship, Marie Curie Cofund, RBUCE-UP No.246556 by the European Commission and PRES UniverSud Paris (Research Based University Chairs of Excellence of Paris). She is one of the Scientific and Technical Committee & Editorial Review Board Member in World Academy of Science, Engineering and Technology, Connecticut, CT 06878, USA.

Rajendra N. Basu is a Chief Scientist and Head, Fuel Cell & Battery Division, Central Glass & Ceramic Research Institute, Kolkata, India. He has obtained his PhD (Materials Science) degree from Indian Institute of Technology, Kharagpur, India. During his professional research career he stayed more than six years in abroad for carrying out his postdoctoral research work in the area of Materials Science & Engineering in the USA (the Pennsylvania State University), Germany (Forschungszentrum Jülich), Japan (Oita University) and Canada (McMaster University). His research interest includes Solid Oxide Fuel Cell, Li-ion Battery, Dense Ceramic Membrane for Gas Separation, Solid Oxide Electrolyser Cell, Energy Materials etc. He is one of the Associate Editors of the Journal, Bulletin of Materials Science and Member of the Editorial Advisory Board of Transactions of Indian Ceramic Society. Dr. Basu received several national and international awards. Dr. Basu is a Fellow of Indian National Academy of Engineering and Member of NASI and other professional societies.